

# Highest methane concentrations in an Arctic River linked to local terrestrial inputs.

Karel Castro-Morales<sup>1\*</sup>, Anna Canning<sup>2</sup>, Sophie Arzberger<sup>1</sup>, Will A. Overholt<sup>1</sup>, Kirsten Küsel<sup>1,3</sup>, Olaf Kolle<sup>4</sup>, Mathias Göckede<sup>4</sup>, Nikita Zimov<sup>5</sup>, and Arne Körtzinger<sup>2,6</sup>

<sup>1</sup> Friedrich-Schiller University Jena, Institute of Biodiversity, Jena, Germany.

<sup>2</sup> GEOMAR Helmholtz Centre for Ocean Research Kiel, Kiel, Germany.

<sup>3</sup> German Centre for Integrative Biodiversity Research (iDiv) Halle-Jena-Leipzig, Germany

<sup>4</sup> Max Planck Institute for Biogeochemistry, Jena, Germany

<sup>5</sup> Pleistocene Park, Northeast Science Station, Chersky, Russia.

<sup>6</sup> Christian Albrecht University Kiel, Kiel, Germany

\*Correspondence: Karel Castro-Morales ([karel.castro.morales@uni-jena.de](mailto:karel.castro.morales@uni-jena.de))

## Abstract.

Large amounts of methane (CH<sub>4</sub>) could be released as a result of the gradual or abrupt thawing of Arctic permafrost due to global warming. Once available, this potent greenhouse gas is emitted into the atmosphere, or transported laterally into aquatic ecosystems via hydrologic connectivity at surface or groundwaters. While high northern latitudes contribute up to 5 % of total global CH<sub>4</sub> emissions, the specific contribution of Arctic rivers and streams is largely unknown. We analyzed high-resolution continuous CH<sub>4</sub> concentrations measured between 15 and 17 June 2019 (late freshet) in a ~120 km transect of the Kolyma River in Northeast Siberia. The average partial pressure of CH<sub>4</sub> (pCH<sub>4</sub>) in tributaries (66.8 – 206.8 µatm) was 2-7 times higher than in the main river channel (28.3 µatm). In the main channel, CH<sub>4</sub> was up to 1600 % supersaturated with respect to atmospheric equilibrium. Key sites along the riverbank and at tributary confluences accounted for 10 % of the navigated transect, and had the highest pCH<sub>4</sub> (41±7 µatm) and CH<sub>4</sub> emissions (0.03±0.004 mmol m<sup>-2</sup> d<sup>-1</sup>) compared to other sites in the main channel, contributing between 14 to 17 % of the total CH<sub>4</sub> flux in the transect. These key sites were characterized by warm waters (T>14.5 °C) and low specific conductivities (κ<88 µS cm<sup>-1</sup>). The distribution of CH<sub>4</sub> in the river could be linked statistically to T and κ of the water, and to their proximity to the shore z, and these parameters served as predictors of CH<sub>4</sub> concentrations in unsampled river areas. The abundance of CH<sub>4</sub>-consuming bacteria and CH<sub>4</sub>-producing archaea in the river was similar to those previously detected in nearby soils, and was also strongly correlated to T and κ. These findings imply that the source of riverine CH<sub>4</sub> is closely related with sites near land. The average total CH<sub>4</sub> flux density in the river section was 0.02±0.006 mmol m<sup>-2</sup> d<sup>-1</sup>, equivalent to an annual CH<sub>4</sub> flux of 1.24×10<sup>7</sup> g CH<sub>4</sub> yr<sup>-1</sup> emitted during a 146-days open water season. Our study highlights the importance of high-resolution continuous CH<sub>4</sub> measurements in Arctic Rivers for identifying spatial and temporal variations, as well as providing a glimpse of the magnitude of riverine CH<sub>4</sub> emissions in the Arctic and their potential relevance to regional CH<sub>4</sub> budgets.

Deleted: The h

Commented [KCM1]: We suggest a change in the title which is more semantically correct

Deleted: r

Deleted: are

Deleted: could

Deleted: potentially

Deleted: formed

Deleted: Upon its release, t

Deleted: can be

Deleted: measured

Deleted: located near

Deleted: ,

Deleted: methane

Deleted: also

Deleted: as well as

Deleted: distance

Deleted: indicators

Deleted: used to predict

Deleted: Similarly,

Deleted: t

Deleted: CH<sub>4</sub>methane -

Deleted: methane

Deleted: suggesting

Deleted: associated

Deleted: close

Deleted: to

Deleted: ies

Deleted: were

Deleted: total

Deleted: .

Deleted:

Deleted: mmol m<sup>-2</sup>

Deleted: variabilities

Deleted: and offers a glimpse to

Deleted: methane

Deleted: methane

## 1 Introduction

Methane (CH<sub>4</sub>) is a powerful greenhouse gas that absorbs the Earth's infrared radiation more efficiently than CO<sub>2</sub>, with a global warming potential 28 times that of CO<sub>2</sub> over a time

horizon of 100 years (Saunois et al., 2020). To date, CH<sub>4</sub> has accounted for 16 to 25 % of the current atmospheric warming (Etminan et al., 2016; IPCC, 2014; Rosentreter et al., 2021).

Globally, aquatic ecosystems contribute about half (53 %) of the total CH<sub>4</sub> emissions, both from anthropogenic and natural origin (Rosentreter et al., 2021). The total bottom-up (i.e., from process-based models and inventories) updated global CH<sub>4</sub> emissions from rivers and streams have a mean of 30.5±17.1 Tg CH<sub>4</sub> yr<sup>-1</sup> (Rosentreter et al., 2021), and account for ~17

% of the average inland water CH<sub>4</sub> fluxes (Saunois et al., 2020). Especially on regional scales, CH<sub>4</sub> emissions from rivers and streams have large impacts on the estimation of local atmospheric emissions (Karlsson et al., 2021). The contribution of CH<sub>4</sub> emissions in high northern latitudes (60 – 90° N) to total global CH<sub>4</sub> emissions ranges between 4 to 5 %, but there are significant uncertainties, particularly regarding the contributions from terrestrial permafrost and non-wetland inland waters, i.e., rivers, streams, and lakes (Saunois et al., 2020). The concentration of CH<sub>4</sub> in rivers and streams is generally above saturation with respect to the present atmospheric CH<sub>4</sub> concentration, emitting annually the equivalent to ~15 % of the total emissions from wetlands or 40 % of the annual CH<sub>4</sub> emissions from lakes (Stanley et al., 2016).

The Arctic Ocean is one of the most river-influenced and land-locked of all the world oceans (Charkin et al., 2017; Shakirov et al., 2020), receiving annually about 10 % of the global runoff (Lammers et al., 2001), through the input from the main six Arctic rivers: Yenisey, Lena, Ob, Mackenzie, Yukon, and Kolyma. These rivers connect the ocean with the land, by mediating the transport of CH<sub>4</sub> stored in terrestrial surface waters or groundwaters, or through soil-water interactions in thawed water tracks (Connolly et al., 2020; Dabrowski et al., 2020; Harms et al., 2020; Saunois et al., 2020). Thus, the riverine transport of soil-derived CH<sub>4</sub> from permafrost may influence the CH<sub>4</sub> concentrations in the Arctic shelf system.

The atmospheric emissions of CH<sub>4</sub> from Arctic inland freshwaters and permafrost have the potential to increase with climate change (Dean et al., 2018). As permafrost thaws, more soil organic carbon is available for the anaerobic degradation of organic matter under warmer conditions, resulting in additional CH<sub>4</sub> formation of which will add to the positive feedback to climate change (Schuur et al., 2015). Trapped or newly formed CH<sub>4</sub> can be emitted directly to the atmosphere after the abrupt or gradual permafrost thaw (Olefeldt et al., 2013; Saunois et al., 2020; Turetsky et al., 2020), or be laterally transported into neighboring inland waters via

Deleted: methane

surface hydraulic connectivity or underground drainage (e.g., Dabrowski et al., 2020). Current and projected changes in the Arctic land surface hydrology, vegetation, landscape, and temperature due to permafrost thaw, will modulate CH<sub>4</sub> concentrations in Arctic fluvial ecosystems (Harms et al., 2020; Olid et al., 2021).

115 The magnitude of the fluvial CH<sub>4</sub> emissions is subject to strong local environmental controls, because CH<sub>4</sub> has low solubility in water (Campeau and del Giorgio, 2014; Stanley et al., 2016). At the same time, the abundance and phylogenetic identity of microorganisms in the river water that can be associated to the formation or consumption of CH<sub>4</sub>, can serve as indicators of the source and fate of CH<sub>4</sub> transported from land. Aquatic CH<sub>4</sub> is subject to  
120 microbial oxidation and photochemical decomposition (Dean et al., 2018; Stanley et al., 2016). Little is known about the magnitude of CH<sub>4</sub> concentrations and emissions from flowing Arctic inland waters, as well as how they vary over time and space. Point CH<sub>4</sub> measurements in some Arctic rivers and streams have demonstrated supersaturation relative to the atmosphere (e.g., Kling et al., 1992; Mann et al., 2022; Striegl et al., 2012; Vorobyev et al., 2021; Zolkos et al., 2019). However, highly resolved aquatic CH<sub>4</sub> measurements are  
125 lacking in large portions of Arctic rivers and streams, and these are needed to better quantify the atmospheric gas fluxes and understand the temporal variations and the environmental indicators. High-resolution measurements of the partial pressure of CH<sub>4</sub> ( $p\text{CH}_4$ ) were measured in a site in Ambolikha River, a tributary of Kolyma River in northeast Siberia,  
130 evidencing aquatic CH<sub>4</sub> supersaturations up of the order of 200 times higher than values at equilibrium with the atmosphere. These measurements allowed identifying temporal variations mostly driven by hydrological changes and air-water exchange, with a consistent decrease of  $p\text{CH}_4$  by 78 % from the measured concentrations during late freshet to summer (Castro-Morales et al., 2022).

135 Here, we present the first high spatial resolution measurements of  $p\text{CH}_4$ , and other complementary water properties, in a large section of the Kolyma River during the late freshet (June) in 2019. Additionally, we followed the riverine microbial community structure using a 16S-amplicon approach along the same 120 km long transect, to provide a potential record of water input sources. The objectives of this study are: 1) to analyze potential environmental  
140 indicators that can be statistically associated with the spatial variations of the  $p\text{CH}_4$  along the sampled river section, 2) to estimate the flux of CH<sub>4</sub> across the atmosphere-river interface, and 3) to investigate a potential link between overall microbial community structure and more specifically the distributions of CH<sub>4</sub> oxidizers and CH<sub>4</sub> producers with the measured  $p\text{CH}_4$  during the sampling period.

Deleted: methane

Deleted: methane

Deleted: methane

## 2 Methods

### 2.1 Study site and fieldwork description

150 The Kolyma River is the sixth largest river in the Arctic, with a watershed area of 653,000 km<sup>2</sup> (Holmes et al., 2012), that is completely underlain by continuous permafrost (Mann et al., 2012). Our area of study was a ~120 km section in the Kolyma River, bounded by the city of Chersky (68° 45' 5.1" N, 161° 18' 16.6" E) to the east and at the location known as Duvanniy Yar (68° 38' 12.8" N, 159° 5' 25.4" E) to the west (Fig. 1). Several floodplains are  
155 located next to the banks of this section of the Kolyma River. These floodplains connect the river to the land during the snow melt period (May and June) when they become inundated. We twice navigated the Kolyma River section onboard a small vessel (average navigation speed of 2.0±0.4 m s<sup>-1</sup>), where we installed our instruments for measurements of continuous water properties and the partial pressure of CH<sub>4</sub> (pCH<sub>4</sub>) (Sect. 2.2.). The first transect was  
160 navigated in the upstream direction (UP) from Chersky to Duvanniy Yar (Fig. 1) between 15 June 2019 (12:48 h; local Chersky time) and 16 June 2019 (16:59 h) (with an overnight break halfway), covering a length of 127.7 km. The second transect was navigated in the downstream direction (DOWN) from Duvanniy Yar to Chersky, and took place between 16 June 2019 (17:00 h) and 17 June 2019 (13:27 h), covering a length of 115.4 km.  
165 In 2019, the ice break-up in Kolyma River at Chersky started on 1 June, and our sampling took place during the late freshet. Thus, during the sampling campaign the transect navigated was completely ice-free and in the decreasing phase of the freshet peak discharge as shown by the daily records from the gauge station Kolymsk-1 (68° 43' 48" N, 158° 43' 12" E) in the Kolyma River (Fig. S1). During the sampling days, the average width of the Kolyma channel  
170 was about 2 km. With help of the Arctic DEM Explorer (Environmental Systems Research Institute, Polar Geospatial Center; <https://livingatlas2.arcgis.com/arcticdemexplorer/>), we estimated a total area of the sampled Kolyma River section of about 221 km<sup>2</sup>. Continuous water properties were measured along both transects (Sect. 2.2). The vessel primarily navigated at the center of the Kolyma River main channel during the sampling,  
175 particularly in the DOWN transect. We purposely navigated in the proximity of the confluences of tributaries and in banks adjacent to floodplains during the UP transect to capture the water properties in regions with visually evident, large lateral contributions from land (i.e., runoff from land as evidenced by more turbid and/or differently colored water). To facilitate the analysis of the high-resolution data and analyze the specific contribution of  
180 banks and confluences with tributaries to the measured water properties and pCH<sub>4</sub>, we defined five key sites (i.e., S1 to S5) that are associated with sampling points along the UP transect.

Deleted: methane

From east to west the location of the “key sites” is: S1, bank of floodplain 1 at Ambolikha river in station PP07; S2, the confluence of tributaries Maly Anyuy and Bolshoy Anyuy (M&B Anyuy) in station PP11; S3, bank of floodplain 2 (only in DOWN transect) in station PP20; S4, bank of floodplain 3 (only in UP transect) in station PP23; and, S5, bank at Duvannyi Yar in station PP25 (Fig. 1). The separation between “key sites” and the “other sites” of the data was done on the basis of the measured  $p\text{CH}_4$ ,  $T$  and  $\kappa$  in the UP and DOWN transects, and also analyzed independently for each transect.

The UP and DOWN transects were not navigated exactly at the same locations and the geographical overlap took place only in a few areas (Fig. 1). Therefore, we compare the results between these transects in the context of the temporal variability of the measured parameters, while the spatial variation is done between the key and other sites of the areas for each transect.

## 2.2 Collection of discrete river water samples and analysis

During the UP transect, we collected discrete water samples at 21 sampling stations (PP05-PP25) distributed along the track (see Fig. 1 for location and Table S1 for sampling times and average water properties measured at each station), for the analysis of total organic carbon (TOC) and the composition of microbial communities (Sect. 2.3.). For this, a 1.5 L Niskin bottle was lowered to 1 m depth and water samples were drawn from the sampler onboard through silicone tubing.

### 2.2.1 Analysis of Total Organic Carbon (TOC) in river water samples

For the quantification of TOC, a volume of 250 mL of water was transferred from the Niskin bottle into an acid-washed amber glass flask. The samples were stored at 4 °C until pre-treatment at the laboratory of the Northeast Science Station in Chersky after the sampling campaign. The samples were brought to room temperature and manually homogenized. Two aliquots of 10 mL were transferred to acid-washed glass vials and acidified to pH 2.0 with 37 % HCl. The samples were kept cold during storage and transport to Germany for the determination of TOC via high-temperature catalytic combustion (Analytik Jena), with each sample measured from three to five times as analytical replicates. Due to the loss of samples, we report results of TOC in water samples from 7 out of 21 stations (33 %).

### 2.2.2 Analysis of microbial communities in river water samples

We determined the distribution and total community composition of microbial communities, including  $\text{CH}_4$ -producing archaea (methanogens) and  $\text{CH}_4$ -oxidizing bacteria (methanotrophs and methylotrophs) in the river water samples. Methanotrophs utilize  $\text{CH}_4$  as carbon source, whereas methylotrophs are more versatile and can also use other C1 compounds as carbon

Deleted: dissolved

Deleted: D

Deleted: Dissolved

Deleted: D

Deleted: D

Deleted: for quantification of DOC

Deleted: filtered through a pre-combusted 0.7  $\mu\text{m}$  GF/F filter (Whatman®). T

Deleted: of the filtrate for each sample

Deleted: D

source. In addition, the abundance of bacteria and archaea was determined along the transects. For this, a volume of 500 mL of the surface river water from the Niskin bottle was transferred into a 500 mL glass flask (DURAN® Borosilicate glass, SCHOTT). Using a hand pump and filtration system, this sample was immediately filtered on board through a 0.2 µm filter (Supor®). The 500 mL were divided into three aliquots and filtered independently for analytical replication. The filters were stored inside 2 mL sterile Biozym tubes and submerged in DNA/RNA shield solution (Zymo Research). The tubes with the filters remained at room temperature for their subsequent transport and analysis in Germany for DNA isolation, amplicon sequencing, and 16S rRNA gene quantification following protocols specified in the supplementing text S.1.2. and S.1.3.

### 2.3 Instrumental setup

Two instruments were installed onboard the vessel for continuous measurements of water properties: (1) an EXO2 multiparameter sonde with seven sensors for simultaneous optical and non-optical water measurements (Sect. 2.3.1), and (2) a Flow-Through (FT) system for continuous measurements of the partial pressure of CH<sub>4</sub> (*p*CH<sub>4</sub>) (Sect. 2.3.2). The instruments were continuously fed with water pumped from the port side of the vessel from a nominal depth of 1 m below the water surface, hereinafter referred to as “surface water”. The surface water was delivered through a PVC tubing of 2.5 m length and split into two outlets: 1) to feed the FT system at an approximate flow rate of 0.14 L s<sup>-1</sup>, and 2) to a 20-L FT box located onboard where the EXO2 probe was immersed for the continuous surface water measurements.

#### 2.3.1 EXO2 Sonde

The EXO2 multiparameter sonde (YSI Inc., Xylem Inc., Yellow Springs, OH, USA) was used to measure optically the turbidity (in formazin nephelometric units, FNU), dissolved O<sub>2</sub> (DO, µmol L<sup>-1</sup>), and fluorescent dissolved organic matter (*f*DOM; Quinine Sulfate Units, QSU) of the incoming surface river water. It also measured temperature-corrected conductivity (specific conductivity,  $\kappa$  in µS cm<sup>-1</sup>) with conductivity electrodes, water temperature (*T*, °C) with a thermistor, and pH with a glass electrode. The sonde had an internal battery and was mounted inside a metal frame (to provide protection and stability) submerged inside the 20 L FT box that received the incoming water pumped from the surface. The bucket was kept covered with a lid to avoid heating of the water and light exposure of the sensors. Considering the same water flow rate at the FT box as in the FT system, the water retention time in the FT box was on average 2.3 min, which allowed a sufficient time for the sensors in the probe to stabilize for a reliable measurement.

The sonde was equipped with a wiper brush that was used routinely to clean the window of the sensors to avoid interferences due to fouling caused by the accumulation of deposits. The wiping periods were registered and removed from the data set. We obtained one measurement every 5 sec and the data was monitored and stored in a computer onboard.

As a result of the travel distance of the pumped water through the pipe (see Sect. S.1.1 for details), the water within the 20 L bucket on board was on average 0.6 °C warmer and with 1.2 mg L<sup>-1</sup> higher DO content than the in-situ water at 1 m depth. Thus, the EXO2 sonde *T* and DO measurements were corrected by these mean values. All the sensors of the sonde were factory-calibrated previous to the measurements. Two-point calibrations were performed on-site to the DO and pH sensors and no analytical drift was observed before and after the measurements that would have required correction. The measured *f*DOM was temperature corrected to a reference of 25 °C (Downing et al., 2012; Watras et al., 2011), and further corrections due to the turbidity influence in the sensor response to light attenuation were done after Snyder et al. (2018).

### 2.3.2 Flow-through (FT) system

The FT system is a portable and versatile flow-through sensor set-up for continuous direct measurements of *p*CH<sub>4</sub> from surface water. We used a [CONTROS HydroC<sup>®</sup> CH<sub>4</sub> FT sensor](#) based on tunable diode laser absorption spectroscopy ([TDLAS](#)) (-4H-JENA engineering GmbH, Jena, Germany). [This sensor has a working accuracy of ±2 µatm or 3 % of the reading](#) (Canning et al., 2021a) [according to the manufacturer standard specifications](#). A SBE45 thermosalinograph sensor (Sea-Bird Electronics, Bellevue, USA) was used to measure the temperature (*T*<sub>FT</sub>, °C) and conductivity of the incoming water. The HydroC<sup>®</sup> CH<sub>4</sub> FT sensor was factory-calibrated before and after the measurement campaign. The calibration and validation of the data were done following Canning et al. (2021a). Drift and response time corrections were not applied because we assume sufficient exposure of the water to the sensor at the low sailing speeds. Because the relatively long response time of the CH<sub>4</sub> sensor (of the order of 20 min), the obtained data are significantly smoothed and therefore, the captured gradients and extreme values might not be precisely geographically located. However, the advantage of the high-spatial-resolution data allowed for a surface coverage that help identify high [CH<sub>4</sub>](#) concentration areas. For more in-depth corrections see Canning et al. (2021a).

Besides the slow navigation speed, the average time spent at each sampling station was 7±13 min (minimum of 2 min and maximum of 8 min), which allowed for further equilibration times of the surface water at the sensors of the instruments, particularly at sites with high

Deleted: methane

Deleted:

CH<sub>4</sub> concentration.

Deleted: methane

We obtained one measurement every 5 sec and the data were monitored and stored on a computer onboard. The EXO2 sonde and FT system data were averaged to 1 min values.

During the measurements, we also navigated inside smaller tributaries, one located at halfway along the transect length (named here as Leonid's stream), and another at the end of the DOWN transect, located along the Ambolikha River. Because the water properties measured in these streams are very contrasting to the properties in the main stem, we removed these sections from the full data, but still present the average values measured along those transects.

## 2.4 CH<sub>4</sub> flux calculation

To obtain the gas exchange across the water-air interface (i.e., flux density) it is necessary to calculate the gas transfer velocities  $k$ . Here we followed two methods to obtain  $k$ : 1) using a hydraulic model as a function of water velocity and discharge, and the river configuration (Raymond et al., 2012), and 2) using a parameterization as a function of wind speed (Wanninkhof, 2014). This was done in order to cover a range of values given the large uncertainties of  $k$  in rivers.

The hydraulic model that we used to calculate  $k$ , is a function of stream velocity ( $V$ , m s<sup>-1</sup>), river slope ( $S$ , unitless), water discharge ( $Q$ , m<sup>3</sup> s<sup>-1</sup>), and water depth ( $D$ , m) (empirical Eq. 7 in Raymond et al., 2012):

$$k_{R12} = 4725 \times (VS)^{0.86} \times Q^{-0.14} \times D^{0.66} \quad (1)$$

The average stream velocity for the transect ( $V=1.27\pm0.1$  m s<sup>-1</sup>) was calculated from the mean daily water discharge from 15 to 17 June 2019 as reported at the gauge station Kolymsk-1 ( $Q=13267\pm950$  m<sup>3</sup> s<sup>-1</sup>) divided by the mean cross-sectional area in the channel

( $A=10400\pm9721$  m<sup>2</sup>).  $A$  was calculated from the average river depth ( $D=5.2\pm4.9$  m) times the river width ( $W$  fixed at 2000 m) at the sampling times. The slope  $S$  for the Kolyma River along the 120 km channel was 0.003 % considering the mean elevation of 4 m, obtained from the slope map in the Arctic DEM Explorer (Environmental Systems Research Institute, Polar Geospatial Center; <https://livingatlas2.arcgis.com/arcticdemexplorer/>). An uncertainty of up to 7.8 % is obtained in this calculation mostly due to the use of an average river depth for the calculation of the cross-sectional area and the stream velocity. The section of the Kolyma River can be in places as shallow as 1.7 m and as deep as 21.6 m, leading to faster water flows as the water column is shallow. However, larger uncertainties are expected due to the variation in  $Q$  along the stream, since the values used here are daily averages measured at once single site at the Kolymsk-1 gauge station.



The empirical wind speed parameterization is used to also calculate  $k$ , followed by Wanninkhof (2014):

$$k_{W14} = 0.251 \times (u_{10})^2 \quad (2)$$

335 Were  $u_{10}$  ( $\text{m s}^{-1}$ ) is the wind speed normalized to 10 m above the water surface, following Amorocho and Devries (1980), calculated from the wind velocities measured at a height of 6 m above ground at a nearby eddy tower during the sampling period (Castro-Morales et al., 2022).

340 The  $k_{R12}$  from the hydraulic model and  $k_{W14}$  from the wind parameterization were standardized to a constant temperature using the Schmidt number ( $Sc$ ) for  $\text{CO}_2$  and freshwater at 20 °C, i.e.,  $Sc_{\text{CO}_2}=600$  (Wanninkhof, 1992), and the  $Sc$  of  $\text{CH}_4$  ( $Sc_{\text{CH}_4}$ ) (Wanninkhof, 2014) following:

$$k_* = k_* \times \left( \frac{Sc_{\text{CH}_4}}{Sc_{\text{CO}_2}} \right)^{-0.5} \quad (3)$$

345 The water-to-air flux density of  $\text{CH}_4$  ( $F$ , amount  $\text{area}^{-1} \text{ time}^{-1}$ ) was obtained with the following function:  $F_* = k_* \cdot (C_w - C_{eq})$ , where  $k_*$  is the gas transfer velocity ( $\text{length time}^{-1}$ ) of  $\text{CH}_4$  at the in-situ  $T$  (Eq. 3) for R12 or W14 (Eq. 1 and 2). The water-side equilibrium concentration of  $\text{CH}_4$  ( $C_{eq}$ ,  $\mu\text{mol L}^{-1}$ ) is subtracted from the measured bulk  $\text{CH}_4$  concentration in the water ( $C_w$ ,  $\mu\text{mol L}^{-1}$ ).  $C_w$  was calculated from the Bunsen solubility coefficient ( $\beta$ ,  $\text{mol L}^{-1} \text{ atm}^{-1}$ ) that is calculated as a function of temperature Weiss (1970), while  $C_{eq}$  was  
350 calculated following Wiesenburg and Guinasso (1979). The atmospheric  $p\text{CH}_4$  ( $\text{atm}$ ) was calculated following:

$$p = x(P - p_{\text{H}_2\text{O}}) \quad (4)$$

where  $x$  is the dry air mole fraction of  $\text{CH}_4$ .  $P$  is the barometric pressure and  $p_{\text{H}_2\text{O}}$  is the saturation water vapor pressure at in-situ water temperature (both in  $\text{atm}$ ). We used the global  
355 mean dry air mole fraction of 1858.8 ppb for  $\text{CH}_4$  during June 2019 according to the Global Monitoring Laboratory, NOAA (Dlugokencky and Tans, 2019), and a standard barometric pressure of 1  $\text{atm}$ .

## 2.5 Data analysis

### 2.5.1 Correlation between water $p\text{CH}_4$ and water parameters

360 To simplify the analysis for finding the relationship between the multiple water parameters measured along the transect and  $p\text{CH}_4$ , we calculated 1-min averages from the continuous measurements of  $T$ ,  $\kappa$ ,  $\text{pH}$ ,  $\text{DO}$ ,  $f\text{DOM}$  and  $p\text{CH}_4$  at the location of the discrete sampling stations in the UP transect. For this analysis, we also included the  $\text{TOC}$  concentrations from seven stations (average  $\pm 1$  std. deviation values are summarized in Table S1), since organic

Deleted: W

Deleted: for this analysis

Deleted: D

Deleted: each

matter can be a source for methanogens. In addition, we calculated the shortest distance from each station ( $z_{\text{stas}}$ ) and of the navigated transects ( $z$ ) to any of the river banks and considered this distance as another parameter relevant for the distribution of  $p\text{CH}_4$  in the river. The river banks along the navigated transects were digitized in Google Earth Pro®, and no other property was used to define the geographical location of these limits; hence, the river banks are fixed locations without temporal variation for the period of our sampling. We obtained  $z_{\text{stas}}$  and  $z$  from the shortest physical distance between the geographical positions of the sampling stations and of the UP and DOWN transects to any of the defined river banks. The river banks and limits of the transect define the polygonal area of interest for this study (Fig. S2).

To find the correlation between the 1-min averages of  $p\text{CH}_4$  and the water properties, as well as the  $\text{T}_{\text{OC}}$  at the sampling stations and  $z_{\text{stas}}$ , we performed a Pearson pairwise linear correlation analysis ( $p < 0.1$ ).

### 2.5.2 Random forest regression analysis for extrapolation of transect $p\text{CH}_4$ into a polygonal area of the river section as a function of $T$ , $\kappa$ and $z$

We estimated the  $p\text{CH}_4$  at the sampling times in the entire river area of a polygon delimited by the river banks and the limits of the navigated transects (Fig. S2). The river bank-forming polygon of the Kolyma River section covered an area of 236.3 km<sup>2</sup>. Within this area we constructed a fine grid regularly distributed within the river polygon and with a horizontal spatial resolution of 0.1 km.

We then built a fine grid polygon in the river for  $T$  and  $\kappa$  based on their best fit correlations to  $z$  at the transect scale, for the “key sites” and for the “other sites” (depending on the measured  $p\text{CH}_4$ ,  $T$  and  $\kappa$ ) at the sampling times during the UP and the DOWN transects. The gridded products were used to extrapolate  $p\text{CH}_4$  to other areas of the river as defined by the gridded area delimited by the river banks, and on the basis of the highly spatially resolved  $p\text{CH}_4$  measured along the transects.

For this, we obtained a best fit between  $T$ ,  $\kappa$  and  $z$  to  $p\text{CH}_4$  by applying a random forest regression analysis. First, for “key sites”, this was done as a function of  $T$  and  $\kappa$ , i.e.,  $p\text{CH}_{4\_key}(T_{\text{key}}, \kappa_{\text{key}})$ . Second, for “other sites” it was done as a function of  $T$ ,  $\kappa$  and  $z$ , i.e.,  $p\text{CH}_{4\_other}(T_{\text{other}}, \kappa_{\text{other}}, z)$ . These models were applied to the gridded polygon to extrapolate  $p\text{CH}_4$  from the transects to the entire gridded polygon. Once a gridded  $T$  and  $\kappa$  was obtained, the corresponding model for  $p\text{CH}_{4\_key}$  and  $p\text{CH}_{4\_other}$  was applied. This procedure was done independently for the UP and DOWN data.

## 3 Results

Deleted: D

### 3.1 Spatial distribution of continuous surface $p\text{CH}_4$ and water properties in UP and DOWN transects

The high-resolution continuous measurements of surface  $p\text{CH}_4$  show significant spatial heterogeneity and temporal variability in both the UP and DOWN transects (Fig. 2). Overall, high  $p\text{CH}_4$  (up to 46  $\mu\text{atm}$ ) was measured in the presence of warm (15.5 °C) and less conductive ( $\kappa < 88 \mu\text{S cm}^{-1}$ ) water, and mostly located closer to the river banks ( $z < 1.0 \text{ km}$ ) (Figs. 3 and 4).

During the UP transect, the average measured  $p\text{CH}_4$  was  $25.8 \pm 6.7 \mu\text{atm}$  (or in terms of  $\text{CH}_4$  concentration,  $C_w = 41.5 \pm 9.2 \text{ nmol L}^{-1}$ ). These values were measured in colder (by 0.6 °C) and less conductive waters (by  $16.1 \mu\text{S cm}^{-1}$ ) compared to the DOWN transect that was navigated two days later. The DOWN transect had on average 7.4  $\mu\text{atm}$  higher  $p\text{CH}_4$  ( $33.2 \pm 9.4 \mu\text{atm}$ , or  $54.3 \pm 14.7 \text{ nmol L}^{-1}$ ) than the UP transect (Table 1 and Fig. 3). In both transects, the concentration of  $\text{CH}_4$  remained supersaturated (by  $1189 \pm 198 \%$  in the UP transect and  $1622 \pm 380 \%$  in the DOWN transect) with respect to the concentration at atmospheric equilibrium (average  $3.2 \pm 0.04 \text{ nmol L}^{-1}$ ).

The spatial distribution of water properties measured in both transects depicted evident differences between the center of the main stem and the areas at the proximity of banks adjacent to floodplains and at confluences of tributaries with the Kolyma main stem (Fig. 2a and 2b, and supplementary Fig. S3). Specifically, hot spots of  $p\text{CH}_4$  with values  $> 35 \mu\text{atm}$  were measured in the key sites at the time of the measurements (Figs. 2 and 3).

During the UP transect, the maximum measured  $p\text{CH}_4$  was 46.1  $\mu\text{atm}$  at site S5 (Duvannyi Yar), very similar to the value measured during DOWN at the same location (i.e., 44.6  $\mu\text{atm}$ ). The maximum  $p\text{CH}_4$  measured in the main stem (80.7  $\mu\text{atm}$ ) was found at a site halfway along the DOWN transect in a site at the outlet of Leonid's stream (location 68.5281 °N, 160.3437 °E). However, the highest  $p\text{CH}_4$  was measured inside streams or tributaries with up to 222.9  $\mu\text{atm}$  at Ambolikha River and up to 92.9  $\mu\text{atm}$  inside Leonid's stream, both navigated during the DOWN transect (Table 1). Larger supersaturations with respect to the atmospheric equilibrium were observed at these two transects with  $9610 \pm 403 \%$  in Ambolikha River and  $3415 \pm 1051 \%$  in Leonid's stream.

In addition to  $p\text{CH}_4$ ,  $T$  and  $\kappa$  were considered to distinguish between the key sites S1 to S5 from the other sites in the river. The key sites S1 to S5 were characterized (besides  $p\text{CH}_4 > 37 \mu\text{atm}$ ) by the presence of warmer ( $T > 14.5 \text{ °C}$ ) and less conductive water ( $\kappa < 88 \mu\text{S cm}^{-1}$ ) at the sampling time. Finally, because the key sites S1 to S5 were evidently located in the proximity of tributary confluences and banks (i.e.,  $z < 0.8 \text{ km}$ ), we also considered  $z$  (distance

to the river bank) as a parameter related to high  $p\text{CH}_4$  in the main stem (Fig. S2 in supplement). The average, minimum and maximum values of  $p\text{CH}_4$ ,  $C_w$ ,  $T$ , and  $\kappa$  in the UP and DOWN transects at “key sites” and all “other sites” of the transect are summarized in Table 1.

Other areas along the transects where  $p\text{CH}_4$  was higher than 37  $\mu\text{atm}$  were not included as part of the key sites because their corresponding  $T$  or  $\kappa$  did not meet the properties specified above, e.g., at the site of the maximum  $p\text{CH}_4$  of 80.7  $\mu\text{atm}$  at the outlet of Leonid’s stream where the  $T = 15.4\text{ }^\circ\text{C}$  and  $\kappa = 113.1\text{ }\mu\text{S cm}^{-1}$  (Figs. 2 and 3).

The pairwise linear correlation analysis ( $p < 0.1$ ) between all the measured parameters showed a statistically significant positive correlation between  $p\text{CH}_4$  and  $T$  ( $r^2 = 0.51$ ), and a negative correlation to  $\kappa$  ( $r^2 = 0.22$ ),  $z_{\text{stas}}$  ( $r^2 = 0.36$ ), and DO ( $r^2 = 0.17$ ). No significant correlation was found between  $p\text{CH}_4$ ,  $f\text{DOM}$  and turbidity.

To analyze if any of the measured water parameters had an influence on the distribution of  $p\text{CH}_4$ , we chose the conservative tracers to which  $\text{CH}_4$  was significantly correlated:  $T$ ,  $\kappa$ , and  $z_{\text{stas}}$ . These conservative parameters are then considered as potential predictors for the presence of dissolved  $\text{CH}_4$  in the river, in contrast to reactive tracers such as DO that can be biologically or chemically altered in the river water. The analysis of environmental indicators was done with the continuous high-resolution data only for the main stem areas.

### 3.2 Influence of conservative tracers on the distribution of riverine $p\text{CH}_4$ along transects and random forest regression as a gap-filling approach

The variations of  $T$  and  $\kappa$  in the river are influenced by the proximity to the outlets of tributaries and the riverbanks. This influence is more evident in the UP transect, where  $T$  and  $\kappa$  at “key sites” correlated positively with  $z$  ( $r^2 > 0.45$ ,  $p = 0.05$ ) (Fig. S4). In the data for the “other sites”, the relation between  $T$  and  $\kappa$  vs.  $z$ , followed a semi-logarithmic fit ( $p = 0.05$ ) in both the UP and DOWN transects (Fig. S5).

To be able to fill gaps and extrapolate the  $p\text{CH}_4$  measured along the transects into the entire polygonal river area, we employed a random forest regression approach based on the correlations between  $T$ ,  $\kappa$  and  $z$ . For this, we first built a fine-gridded polygon for  $T$  and  $\kappa$  using the linear (for “key sites”) and semi-logarithmic correlations (for “other sites”) observed at the transect level during the sampling times. Once a gridded  $T$  and  $\kappa$  were generated, the corresponding random forest model for  $p\text{CH}_{4\_key}$  and  $p\text{CH}_{4\_other}$  at transect level as a function of  $T$ ,  $\kappa$  and  $z$  correspondingly, was applied. This procedure was done independently for the UP and DOWN transects, hence two polygons representing the modeled  $p\text{CH}_4$  during 15–16 June 2019 and 16–17 June 2019 were obtained (Fig. S6).

To validate the output of the random forest models, we compared the measured and modeled  $p\text{CH}_4$  along each transect. Results show that the skill of the model for the UP transect better reproduces the  $p\text{CH}_4$  with an uncertainty of 3.9  $\mu\text{atm}$  than that of the model for the DOWN transect (uncertainty of 9.1  $\mu\text{atm}$ ) (Fig. S7). A larger error is observed in the areas of the key sites mostly during the DOWN transect.

### 3.3 Microbial composition and **TOC** analysis in discrete water samples

Similar to the influences of temperature ( $T$ ) and specific conductivity ( $\kappa$ ) on the distribution of  $p\text{CH}_4$ , we found that microbial community composition was significantly related to both  $T$  ( $F = 15.5$ ,  $r^2 = 0.17$ ,  $p < 0.001$ ) and specific conductivity ( $\kappa$ ) ( $F = 12.7$ ,  $r^2 = 0.14$ ,  $p < 0.001$ ) (Fig. 5), while distance to the shore ( $z$ ) was not significant. The  $p\text{CH}_4$  measurements alone explained a low portion of the community variance ( $r^2 = 0.06$ ,  $p < 0.03$ ), and when tested in conjunction with both  $T$  and  $\kappa$ , was not a significant contributor to microbial community variance. In this way, microbial community composition can act as a record of  $p\text{CH}_4$ , as microbes – and  $T/\kappa$  – are less dynamic than  $p\text{CH}_4$ . Within the context of the strong patterns related to both  $T$  and  $\kappa$ , there were spatial patterns that reflected the location within the main stem and the influences of tributaries, with key site S3 (PP20) exhibiting the lowest similarities with the other four key sites and clustering with other water samples collected within the main stem of the river. Conversely, key sites S1 and S2 clustered separately from all other water samples, likely due to the heavy influence of tributary outflow and floodplain inputs (Fig. 5).

Quantifying the 16S rRNA gene abundances of total archaeal and bacterial populations revealed that archaea, were three orders of magnitude lower in abundance than their bacterial counterparts across the river transect. However, the abundances of both were found to strongly correlate (Pearson,  $r^2 = 0.81$ ,  $p < 1.8\text{e-}15$ ) (Supplemental Fig. S8). Within the archaeal 16S sequences detected, we found two putatively methanogenic OTU, each belonging to a different family/genus (*Methanobacteriaceae* – *Methanobacterium*, *Methanoregulaceae* – *Methanoregula*). The highest relative abundance of methanogens (0.012 %) occurred within station PP07 (key site S1) (Fig. 6a), and the other key sites with the highest  $\text{CH}_4$  concentrations did not exhibit particularly elevated methanogens abundances. Conversely, bacterial putative groups associated with methanotrophy/methylotrophy, particularly OTU within the family *Methylophilaceae*, were detected at all sites and ranged between 3.5 to 5.5 % relative abundance (Fig. 6b). Restricting our analysis to genera known to be strict methanotrophs, we find sequences affiliated with *Methylobacter* that range from 0.01 – 0.3 % relative abundance, and only traces of *Ca. Methanoperedens* (Supplemental Fig.

Deleted: D

S9). The relative abundances of these groups were approximated to pseudo-absolute abundances using the quantitative qPCR results from each sample. Patterns in methanogen abundances were consistent regardless of scale (Fig. 6c), while methano-/methylotrophs exhibited higher abundances within stations PP10, PP11 (key site S2), and PP23-PP25 (incl. key sites S4 and S5), and lower abundances within PP06, PP09, PP15, PP17, and PP20 (key site S3) (Fig. 6d). As this data is based only on DNA analyses, a distinction between active and dead cells is not possible.

The correlations between the total absolute abundances of archaeal microbial communities against the water properties at stations (Fig. 7) show statistically significant ( $p < 0.05$ ) positive linear correlations between  $T$  and the abundance of methanogens ( $r^2 = 0.35$ ,  $p = 0.005$ ) and methano-/methylotrophs ( $r^2 = 0.43$ ,  $p = 0.001$ ) (Figs. 7a and 7b). A statistically significant negative linear correlation was obtained against  $p$  ( $r^2 = 0.31$ ,  $p = 0.007$ ) for methanogens and for methano-/methylotrophs ( $r^2 = 0.24$ ,  $p = 0.02$ ) (Figs. 7c and 7d). The  $pCH_4$  at stations is also positively correlated and statistically significant (at  $p < 0.05$ ) to the abundance of methano-/methylotrophs ( $r^2 = 0.22$ ,  $p = 0.04$ ), but is not statistically significant when correlated with methanogens (Figs. 7e and 7f).

The average TOC measured in 7 out of the 21 sampling stations was  $7.5 \pm 0.7$  mg L<sup>-1</sup> (Table S1). Since organic matter in suspension can be an important carbon source for methanogens, we correlated TOC v  $pCH_4$ . A negative but not significant correlation at  $p < 0.1$  was found between  $pCH_4$  and TOC.

### 3.4 Surface CH<sub>4</sub> emissions at transects and polygonal surface area at the Kolyma River section

The average gas transfer velocity during the sampling period was calculated with a hydraulic model ( $k_{R12} = 0.5 \pm 0.02$  m d<sup>-1</sup>) and a wind speed parameterization ( $k_{W14} = 0.4 \pm 0.3$  m d<sup>-1</sup>) are in close agreement. Because the magnitude of the flux density of CH<sub>4</sub> calculated in both transects with these two  $k$  values does not differ considerably (i.e.,  $F_{R12} = 0.02 \pm 0.007$  mmol m<sup>-2</sup> d<sup>-1</sup> and  $F_{W14} = 0.01 \pm 0.01$  mmol m<sup>-2</sup> d<sup>-1</sup>), we chose to present only  $F_{R12}$  calculated using  $k_{R12}$  after the hydraulic model.  $F_{R12}$  will be presented hereinafter to as the flux density of CH<sub>4</sub>, FCH<sub>4</sub>.

The average FCH<sub>4</sub> of CH<sub>4</sub> along the UP transect was  $0.019 \pm 0.005$  mmol m<sup>-2</sup> d<sup>-1</sup> and along the DOWN transect was  $0.026 \pm 0.008$  mmol m<sup>-2</sup> d<sup>-1</sup>. Maximum FCH<sub>4</sub> values at key sites were  $0.034$  mmol m<sup>-2</sup> d<sup>-1</sup> for site S5 during the UP transect, and  $0.045$  mmol m<sup>-2</sup> d<sup>-1</sup> at the key site S2 during the DOWN transect (Fig. 3). Average FCH<sub>4</sub> in both transects was 1.5 times higher at key sites than in the other sites of the transects (Fig. 8). This is relevant considering that the

Deleted: a

Deleted: |

Deleted:  $r^2 = 0.24$

Deleted: ( $r^2 = 0.11$ ) and methano-/methylotrophs ( $r^2 = 0.21$ )

Deleted: D

Deleted: all

Deleted: of the

Deleted: 9.0

Deleted: 1.0

Deleted: . The largest DOC values were measured at some of the sampling stations located on the east side of the transect at the confluence between tributaries and the Kolyma main stem or closer to the river bank. The highest measured DOC value was  $11.9$  mg L<sup>-1</sup> at station PP05, located at the confluence between the Panteleikha-Ambolikha rivers and the Kolyma main stem, whereas the lowest DOC value was measured at station PP25 near the river bank at Duvannyi Yar ( $7.5$  mg L<sup>-1</sup>) despite the large turbidity observed in this site. Other sampling stations located at confluences or near banks reached values  $\geq 9$  mg L<sup>-1</sup>, i.e., PP07 and PP10 close to the riverbank, PP18 and PP19 located inside and outside Leonid's stream respectively, as well as station PP11 at the confluence to the Maly and Bolschoi Anjui (M&B Anjui) tributaries ...

Deleted: and Fig. S10

Deleted: No

Deleted: (

Deleted: )

Deleted: D

Deleted: 7

surface area represented by the key sites is 8 to 12 times smaller than the rest of the transects (calculated considering the navigated distance times a radius of 50 m around the sampling point).

The ~~area integrated~~ CH<sub>4</sub> flux ~~in the~~ UP transect (~~1.27×10<sup>6</sup> m<sup>2</sup>, considering its reach length of 127.7 km times an arbitrary 10 m radius of influence~~) was ~~2.4×10<sup>4</sup> mmol d<sup>-1</sup>~~. Taking into account ~~only the area of~~ key sites in the UP transect (~~1.06×10<sup>5</sup> m<sup>2</sup>~~) and the emissions in these areas (~~0.032 mmol m<sup>-2</sup> d<sup>-1</sup>~~), the key sites in the UP transect contributed to 14 % (~~3,392 mmol d<sup>-1</sup>~~) of the ~~total area integrated emissions in the entire transect~~. In the DOWN transect, the ~~integrated~~ CH<sub>4</sub> flux was ~~2.9×10<sup>4</sup> mmol d<sup>-1</sup>~~ (area of ~~1.15×10<sup>6</sup> m<sup>2</sup>, considering 115.4 km of reach length times the 10 min radius~~). The key sites of the DOWN transect covered an area of ~~1.37×10<sup>5</sup> m<sup>2</sup>~~ and the CH<sub>4</sub> emissions in these areas were ~~0.036 mmol m<sup>-2</sup> d<sup>-1</sup>~~, resulting in a ~~contribution of 17 % (4,932 mmol d<sup>-1</sup>) of the total area integrated emissions of the entire DOWN transect~~.

We also calculated FCH<sub>4</sub> for a smaller stream (Leonid's stream) and the Ambolikha River (second-order tributary of Kolyma River) (Fig. 1), that were navigated during the DOWN transect on 17 June 2019. These navigated sections were not included in our estimate for main channel. The average FCH<sub>4</sub> at the Ambolikha River (~~0.17±0.008 mmol m<sup>-2</sup> d<sup>-1</sup>~~) and at the Leonid's stream (~~0.05±0.02 mmol m<sup>-2</sup> d<sup>-1</sup>~~) were nearly five and two times higher respectively than at the key sites of the main channel during the DOWN transect (Fig. 8).

Based on the modeled *p*CH<sub>4</sub> in the gridded surface area of the Kolyma River section, we calculated the corresponding FCH<sub>4</sub> that would have been emitted through the total surface of the river section (~~236.3 km<sup>2</sup>~~), ~~and not only at the transect locations~~. The total CH<sub>4</sub> flux at the surface of the river section during the UP transect is calculated as ~~4.5×10<sup>6</sup> mmol d<sup>-1</sup>~~ (or ~~7.2×10<sup>4</sup> gCH<sub>4</sub> d<sup>-1</sup>~~), and for the DOWN transect is ~~6.1×10<sup>6</sup> mmol d<sup>-1</sup>~~ (or ~~9.8×10<sup>4</sup> gCH<sub>4</sub> d<sup>-1</sup>~~) emitted through the surface of the Kolyma River section during the sampling time of both transects (15-17 June 2019).

## 4 Discussion

### 4.1 Patterns and indicators of the spatial distribution of CH<sub>4</sub> in Kolyma River and associated tributaries and streams

In June 2019, the Kolyma River exhibited large *p*CH<sub>4</sub> values that were up to 1,300 % supersaturated (equivalent to 28.3±8.5 μatm) with respect to atmospheric equilibrium. These values are comparable to measurements reported for summer in the main channel of the Lena River, i.e., 18 to 51 μatm, calculated from 30 to 85 nmol L<sup>-1</sup> for a *T*=14 °C in freshwater; (Bussmann, 2013). However, a large range in *p*CH<sub>4</sub> values has been measured in other Arctic

Deleted: cumulative

Deleted: sum of the

Deleted: es

Deleted: in the

Deleted:

Deleted: for the period of sampling (1 day) was 14.4 mmol m<sup>-2</sup>...

Deleted:

Deleted: At

Deleted: , the fluxes accounted for 13 % (1.8 mmol m<sup>-2</sup>) of the total flux.

Deleted: total

Deleted: 10.5 mmol m<sup>-2</sup>

Deleted: , and the contribution of the key sites to the total emissions increased to 20 % (2.1 mmol m<sup>-2</sup>)

Deleted: .

Deleted: 7

Deleted: 934.2

Deleted: 1.1

Deleted: <sup>4</sup>

Deleted: m

Deleted: C

Deleted: 1391.9

Deleted: 1.7

Deleted: <sup>14</sup>

Deleted: m

Deleted: C

Deleted: ). This estimation allows for the calculation of the flux of gas through the entire surface area of the river section (and not only at the transect locations). We estimated an average of 3.3×10<sup>12</sup> mgC d<sup>-1</sup> (equivalent to 3300 tC d<sup>-1</sup>) of the total CH<sub>4</sub>

Deleted: methane

Rivers, such that the average  $p\text{CH}_4$  in the Kolyma River is three times higher than measurements at the main channel of the Yukon River in North America (8.4  $\mu\text{atm}$ ) (Striegl et al., 2012), and almost nine times lower than the mean  $p\text{CH}_4$  value (236  $\mu\text{atm}$ ) in surface waters of Kuparuk River in Alaska (Kling et al., 1992).

Our highly spatially-resolved underway continuous measurements of surface dissolved  $\text{CH}_4$  were pivotal to reveal spatial variabilities and features in the main river channel that cannot be obtained with sparse discrete sampling. The surface distribution of  $p\text{CH}_4$  measured in a ~120 km section of Kolyma River was heterogeneous, with nearly two-fold higher concentrations observed along riverbanks and near the confluence of tributaries (69  $\text{nmol L}^{-1}$ , or  $p\text{CH}_4=41.1 \mu\text{atm}$ ) than at the central parts of the river (46  $\text{nmol L}^{-1}$ , or  $p\text{CH}_4=27.8 \mu\text{atm}$ ) (Fig. 2 and Table 1). Previous studies have demonstrated the influence of land to the distribution of riverine  $\text{CH}_4$  concentrations, for example along the Danube River (Canning et al., 2021b), and within the Lena River (Bussmann, 2013). The concentration of dissolved  $\text{CH}_4$  in Arctic sites with direct contact to adjacent lands, such as in small tributaries, streams, lakes channels or ponds, has been shown to be two to five times higher than what is observed in the main stems of large rivers (Bussmann, 2013; Dean et al., 2020; Kling et al., 1992; Striegl et al., 2012). In samples from creeks draining from permafrost into the Lena River,  $\text{CH}_4$  concentrations (1505  $\text{nmol L}^{-1}$ , or  $p\text{CH}_4$  of 900  $\mu\text{atm}$ ) were between twenty to fifty times higher than in fluvial waters (Bussmann, 2013). At the Lena Delta, the concentrations of  $\text{CH}_4$  are higher (212  $\text{nmol L}^{-1}$ , or  $p\text{CH}_4$  of 114.7  $\mu\text{atm}$ ,  $T=9.8^\circ\text{C}$  and  $S=2.45$ ), because they were directly influenced by bottom soils (Bussmann et al., 2017). In tributaries of the Yukon River, the  $\text{CH}_4$  concentrations were up to 690  $\text{nmol L}^{-1}$ , being two times higher than in the main stem of the same river (290  $\text{nmol L}^{-1}$ ) (Striegl et al., 2012). Similarly, our results show that, besides the in-stream variability, tributary or stream  $\text{CH}_4$  concentrations measured at the Ambolikha River and Leonid's stream, were between two to six times higher than those in the main channel of Kolyma River.

The average  $p\text{CH}_4$  measured at the Ambolikha River ( $206.8 \pm 9.8 \mu\text{atm}$ ) is consistent with the measurements at the Kuparuk River (236  $\mu\text{atm}$ ) (Striegl et al., 2012), and the mean  $p\text{CH}_4$  ( $292 \pm 109 \mu\text{atm}$ ) measured during a 38-day time-series study that started 9 days after the present study (i.e., on 26 June 2019) at a site in the Ambolikha River (Castro-Morales et al., 2022). Whereas the average  $\text{CH}_4$  concentration measured at Leonid's stream was 67  $\mu\text{atm}$  (111 nM), which is in the same order of magnitude as the maximum value measured at the plume of Kolyma River at the East Siberian Arctic shelf in the summer of 2004 (55  $\mu\text{atm}$ , obtained from the reported 110 nM,  $T=5^\circ\text{C}$  and  $S=14$ ) (Shakhova and Semiletov, 2007).



We characterized the spatial distribution of riverine  $p\text{CH}_4$  as a function of temperature ( $T$ ), specific conductivity ( $\kappa$ ) and the distance from the river banks ( $z$ ), as suitable indicators for the distribution of  $\text{CH}_4$  during the late spring over larger areas of the Kolyma River (and potentially applicable to other Arctic rivers). We found that the distance to river banks is an indicator of the proximity to potential terrestrial  $\text{CH}_4$  sources, hence it can be a useful benchmark for understanding the distribution and fate of  $\text{CH}_4$  in natural surface waters (Fig. 4). With a statistical approach, we used the selected predictors to fill gaps in areas of the river where no  $\text{CH}_4$  data were available (Fig. S6). Similar approaches could be used to improve the  $\text{CH}_4$  data currently available for the global  $\text{CH}_4$  budget (Saunois et al., 2020) and to aid in forecasting riverine  $\text{CH}_4$  following the projected increases in warmer river waters, abrupt permafrost thawing, and collapse of riverbanks.

#### **4.2 Identification of microbial communities associated with the riverine $\text{CH}_4$ concentrations**

Overall patterns in microbial community composition, e.g., the similarities in the relative abundances of bacterial and archaeal groups, were also strongly related to the temperature and specific conductivity of the river water (Fig. 5). Unlike with  $\text{CH}_4$ , distance to shore was not apparent in explaining differences in community composition. Arctic riverine microbial communities track closely with water temperature, flow rate, and biogeochemistry (Campeau and del Giorgio, 2014; Crump et al., 2009) and match patterns in DOM composition and concentration (Castro-Morales et al., 2022; Kaiser et al., 2017). The strong explanatory power of temperature and specific conductivity we observe in this study fits in with the concept of riverine community coalescence as they approximate the mixing of distinct water sources over a spatially small region, whereby the dynamic community assemblage mechanisms are inextricably linked to transport processes and rapidly changing selective pressures (Mansour et al., 2018). In this sense, spatial patterns in community composition can act as robust bioindicators of the relative inputs of transported metabolic end products derived from terrestrial sources, like  $\text{CH}_4$  or  $\text{CO}_2$ . To support the relationship between community composition and the originating source of  $\text{CH}_4$ , we examined the distributions of functional microbial groups putatively associated with  $\text{CH}_4$  production and consumption. The strongest evidence was the overlap in detected methanotrophs and methanogens within our study and a previous study by Kwon et al. (2017), that examined these groups within permafrost soils adjacent to our site (PP09). More specifically the highest relative abundances of groups associated with *Methanobacterium* and *Methylobacter* in both the surficial soils and our discrete water samples.

Expanding on this, biological CH<sub>4</sub> production has traditionally been assumed to occur only in anoxic environments, and methanogens, as strict anaerobes, are unsuited to grow within oxic river waters. Our data shows that river water was oxic at all stations with an average O<sub>2</sub> saturation of 110 %, which should preclude methanogenesis. However, there is increasing evidence that there is CH<sub>4</sub> production in oxic marine and freshwaters, and a link between oxic *in situ* production of CH<sub>4</sub> and algal dynamics (i.e., photosynthesis and respiration rates) (Bogard et al., 2014). Oversaturation of CH<sub>4</sub> in oxic surface waters of lakes can also result from CH<sub>4</sub> release from littoral sediments in combination with horizontal transport to the open water. The relative importance of both processes is under debate (Bogard et al., 2014; Encinas Fernández et al., 2016; Grossart et al., 2011; Peeters and Hofmann, 2021). The second process also explains better the higher CH<sub>4</sub> concentrations observed in shallow zones compared to deep waters of lakes (Peeters and Hofmann, 2021). For the Kolyma River, we propose that the oversaturated CH<sub>4</sub> concentrations located close to the river bank and at confluences with tributaries, and the presence of methanogens, is mainly caused by the lateral release of CH<sub>4</sub>-rich pore water and soil-borne methanogens. This process might be dominant during permafrost melting and resuspension events, rather than *in situ* net production of CH<sub>4</sub> in oxic surface waters by active methanogens. The relative and pseudo-absolute abundances of sequences affiliated with methanogens further act as more specific indicators of sources originating from anoxic, terrestrial CH<sub>4</sub> hotspots, as supported by the statistically significant correlation between methanogen abundance and CH<sub>4</sub> concentration (Fig. 7). Additionally, we anticipate that the methanogenic archaea exhibit longer residence times than CH<sub>4</sub> itself due to its high diffusion and oxidation rates. The presence of soil-derived methanogens in the river water might be indicative of even higher riverine CH<sub>4</sub> concentrations, as part of it can be already outgassed or oxidized. The weaker correlation of CH<sub>4</sub> to methanogen abundance compared to temperature or specific conductivity, parameters expected to change slower than CH<sub>4</sub> concentrations, likely reflects these differences in transport mechanisms. Of the two methanogens we detected, *Methanobacterium* was recently shown to be the primary methanogen detected in the surface waters of thermokarst ponds and is more typical of acidic and peat-dominated aquatic ecosystems (Vigneron et al., 2019). *Methanoregula* (within order *Methanomicrobiales*) have also been shown to be abundant groups within permafrost thaw lakes (Crevecoeur et al., 2016) and were suggested to be more typical of deeper and less acidic water bodies (Vigneron et al., 2019) (Fig. 6). Conversely, we expected microbial groups that consume CH<sub>4</sub> to also be indicative of CH<sub>4</sub> sources into the river. Groups affiliated with methylotrophy (e.g., *Methylophilaceae* –

Deleted: is only known from the Archaeal domain of life,

Deleted: ,

Deleted: (Evans et al., 2019)

Deleted: methane

Deleted: methane

Deleted: methane

*Methylothera*) exhibited ten times higher relative abundances than groups of strict methanotrophic organisms (*Methylobacter*) (Fig. 6), suggesting that in addition to  $\text{CH}_4$ , other sources like methanol associated to the degradation of  $\text{CO}_2$  by methanotrophs (Xin et al., 2007) or by some groups of phytoplankton (Mincer and Aicher, 2016), were sources of carbon in this environment. In support of this finding, aerobic methanotrophs have been found at much higher relative abundances (>25 %) and higher diversity within thermokarst well-stratified subarctic Canadian ponds, than the maximum of 0.3 % detected here, where distinct genera (*Methylobacter* and *Methylomonas*) within the order *Methylococcales* where the most abundant (Crevecoeur et al., 2015; Vigneron et al., 2019). This is a sensical finding, as the dynamic river flow enables the diffusive  $\text{CH}_4$  transport and emissions to the atmosphere compared to the emissions across smaller surface areas in highly-stratified, less dynamic and largely anoxic pond environments. The majority of the  $\text{CH}_4$  produced in thawing permafrost is first locally oxidized before it can be released to the atmosphere (Olid et al., 2021). Thus, the higher relative abundance of  $\text{CH}_4$ -consuming bacteria compared to  $\text{CH}_4$ -producing archaea in the Kolyma River suggests that a considerable fraction of  $\text{CH}_4$  is already oxidized within the recently thawed active layer.

#### 4.3 Temporal variability of $\text{CH}_4$ in Kolyma River

Our continuous high-resolution measurements of  $p\text{CH}_4$  in the Kolyma River allowed us also to identify a large temporal variability in spite of the short time scale of our measurements. The differences in the  $p\text{CH}_4$  and  $\text{FCH}_4$  (flux density of  $\text{CH}_4$ ) between the UP and DOWN transects might be due to a rapid response to changes in  $\text{CH}_4$  driven by the interactions between the main flow of the river and the continuous contribution of external  $\text{CH}_4$  inputs resulting from melting, rather than by an advective signal travelling down the main channel of Kolyma River. Still, our measurements cannot represent any mid- to long-term  $\text{CH}_4$  variation in the river, and the differences between the transects might also be due to different spatial locations.

The Kolyma River Basin is the only one in the Arctic completely underlain by continuous permafrost, which could result in even higher soil  $\text{CH}_4$  production and release into the river network during permafrost thaw compared to other Arctic rivers. During the Arctic melt season (May to June), the surface hydrologic connectivity between the land and rivers is enhanced. As the seasonal progression takes place, deeper water-saturated soil layers are thawed, and substances, microorganisms, and gases, like  $\text{CH}_4$ , are mobilized through the lateral transfer from groundwater discharge into Arctic inland waters, particularly to the fluvial network (Connolly et al., 2020; Harms et al., 2020; Saunois et al., 2020). It has been

Deleted: methane

Deleted: methane

Deleted: methane

Deleted: methane

785 demonstrated that the majority of the CH<sub>4</sub> emitted to the atmosphere from subarctic ponds is sustained by the discharge of CH<sub>4</sub> from groundwaters upon the active layer thaw (Olid et al., 2021).

#### 4.4 CH<sub>4</sub> emissions in Kolyma River and comparison to other estimates

The average estimated annual flux in the polygon section at the Kolyma River during our sampling is  $1.24 \times 10^7$  g CH<sub>4</sub> taking into account a polygon surface area of 236.3 km<sup>2</sup> and 146-days ice-free season (between 20<sup>th</sup> May and 12<sup>th</sup> October 2019 obtained from the river discharge curve, Fig. S1). This calculation is by far from robust and largely uncertain, considering that our measurements only correspond to a short-term data set during the open water season, and that large temporal and spatial variations in relation to e.g., changes in water sources, temperature regime and lateral carbon inputs throughout the ice-free period is expected. This has been recently demonstrated at the Ambolikha River (tributary of the Kolyma River), where riverine CH<sub>4</sub> concentrations decreased over time during the open water season due to persistent emissions to the atmosphere dominating over declining external gas inputs during the summer low flow (Castro-Morales et al., 2022). Thus, the annual CH<sub>4</sub> flux value provided here for the investigated Kolyma River section, provides an upper end of the potential magnitude and relevance of CH<sub>4</sub> atmospheric emissions from an Arctic River. Despite the large uncertainty, our estimated CH<sub>4</sub> emissions are four orders of magnitude smaller than the annual flux of CH<sub>4</sub> at the East Siberian Arctic Shelf (ESAS) estimated to be  $0.11 \times 10^{12}$  g CH<sub>4</sub> yr<sup>-1</sup> (or 0.11 Tg CH<sub>4</sub> yr<sup>-1</sup>, for a 90-days ice-free season) in summer of 2003 and 2004 for a surface area of  $1.0 \times 10^6$  km<sup>2</sup> (which is orders of magnitude greater than the polygon section of Kolyma River) (Shakhova and Semiletov, 2007). In Arctic shelves, the concentration of CH<sub>4</sub> is strongly influenced by riverine inputs, particularly in bottom layers of shelf waters due to differential water density gradients (Shakhova and Semiletov, 2007). Decreasing flow velocities (i.e., discharge) allow the sedimentation of organic matter in the delta areas, stimulating microbial sedimentary processes that finally lead to the formation of CH<sub>4</sub> and CO<sub>2</sub>. Dropping water levels during summer also facilitates CH<sub>4</sub> emissions from riverine sediments to the atmosphere. This has been observed in the Lena River region, where contributions from bottom surface sediments are more significant to the measured CH<sub>4</sub> concentrations than riverine lateral exports (Bussmann et al., 2017). As both the oxidation rates and the diffusive emissions of CH<sub>4</sub> through the water-atmosphere interface are faster processes than the lateral gas transport in the water column. Thus, despite the large CH<sub>4</sub> concentrations and emissions identified in the upstream river waters, the surface riverine CH<sub>4</sub> measured >100 km upstream of the shelf is locally emitted (or oxidized) and

Deleted: Methane

Deleted: 0.63

Deleted: <sup>12</sup>

Deleted: yr<sup>-1</sup> (or 0.63 Tg CH<sub>4</sub> yr<sup>-1</sup>)

Deleted: ,

Deleted: for a

Moved (insertion) [1]

Deleted: considering a surface area of 236.3 km<sup>2</sup>

Formatted: Font colour: Text 1

Formatted: Subscript

Deleted: on the same

Deleted: as

Deleted: to

Deleted: This calculation is by far robust and largely uncertain, considering that our measurements only correspond to a short-term data set during the open water season, and that large temporal and spatial variations in relation to e.g., changes in water sources, temperature regime and lateral carbon inputs throughout the ice-free period is expected. This has been recently demonstrated at the Ambolikha River (tributary of the Kolyma River), where riverine CH<sub>4</sub> concentrations decreased over time during the open water season due to persistent emissions to the atmosphere dominating over declining external gas inputs during the summer low flow (Castro-Morales et al., 2022) the annual CH<sub>4</sub> flux value provided here for the investigated Kolyma River section, provides an upper end of the potential magnitude and relevance of CH<sub>4</sub> atmospheric emissions from an Arctic River.

Moved up [1]: (Castro-Morales et al., 2022)

845 does not influence the surface CH<sub>4</sub> concentrations measured at the river plume and at the East Siberian Arctic Shelf.

Morphology and stream size seem to be also key parameters for the amount of gas delivered from land and emitted through the water surface into the atmosphere, as the potential for large gas emissions is higher in smaller streams with shorter water travel distances. Our data  
850 support this assumption, as the FCH<sub>4</sub> at key sites was two to five times lower than the average FCH<sub>4</sub> at the smaller Leonid's stream and Ambolikha River respectively (Fig. 8). The surface areas of the key sites characterized by elevated FCH<sub>4</sub> are between 8 to 12 times smaller than the surface area covered by the rest of the transect. However, the CH<sub>4</sub> emissions at key sites were 1.5 times higher than in the other sites, and represent between 13 to 20 % of the total  
855 cumulative emissions in both transects.

Because the diffusion of CH<sub>4</sub> in water is slower than in air, riverbanks can thus act as efficient vectors for the local emissions of CH<sub>4</sub> formed and stored in the subsoil. The projected increase in freshwater inputs, deepening of active layers, and increase in soil drainage, as more permafrost is thawing in response to warmer and wetter Arctic summers (AMAP, 2017; Bring et al., 2016; Bussmann et al., 2017; Chiasson-Poirier et al., 2020), will enhance the  
860 input of CH<sub>4</sub> from external terrestrial sources at hotspots over extended periods during the open water season. Additionally, projected longer ice-free periods in the Arctic, i.e., an earlier start of melt periods and longer open water seasons, can therefore lead to an increase in CH<sub>4</sub> emissions from inland waters (Wik et al., 2016). This ultimately will have an impact on the  
865 current CH<sub>4</sub> budget of the Arctic. By not considering the variable aquatic ecosystems and water cycle of the Arctic, the estimated 4 to 5 % contribution of high latitudes to the total global CH<sub>4</sub> emissions (Rosentreter et al., 2021; Saunois et al., 2020) may be underestimated.

The irregular location of CH<sub>4</sub> hot spots along the river banks and their potentially continuous elevated CH<sub>4</sub> contributions to the river, possess a challenge to estimating lateral transport of  
870 CH<sub>4</sub> from upstream to downstream waters. Elevated CH<sub>4</sub> concentrations at the Arctic shelves are thus primarily influenced by local sources (i.e., bottom soils and degrading shelves) (Shakhova and Semiletov, 2007). However, to improve the estimates of riverine CH<sub>4</sub> concentrations that can actually reach the ocean in the context of increasing warming and thawing, and to improve the knowledge of the contribution of Arctic rivers and streams to the  
875 regional and global CH<sub>4</sub> budgets, it is necessary to intensify the spatial and temporal resolution of the direct measurements of CH<sub>4</sub> in Arctic Rivers.

Deleted: methane

## 5 Conclusions

880 In this study, we measured for the first time continuous high-resolution  $p\text{CH}_4$  in a large section of Kolyma River during the late freshet of 2019, and combined these observations with microbial community analysis in water samples to investigate the potential source of this gas. The large spatial variability of surface  $\text{CH}_4$  concentrations in the river channel was associated with hotspots located at the river bank and at confluences with tributaries where

885  $\text{CH}_4$  was almost two times higher than at the center of the channel. The identified presence of  $\text{CH}_4$ -producing archaea in a well oxygenated river water suggests that most of the  $\text{CH}_4$  is laterally transported from external terrestrial sources into the river channel, rather than produced within the river water. Elevated riverine local  $\text{CH}_4$  emissions were associated with identified hotspot areas on land suggesting efficient linkages between the land and the aquatic

890 ecosystems. Our analysis does not reveal the reach length of the  $\text{CH}_4$  measured from our site to downstream waters. We suggest that the  $\text{CH}_4$  measured in waters 100 km upstream the Arctic Ocean, might not reach shelf waters and instead is locally emitted to the atmosphere or oxidized in the river course. For this specific purpose, future works should include stable isotope studies to trace the sources and pathways of the  $\text{CH}_4$  in the river water. Without

895 continuous measurements, it will remain unclear how much  $\text{CH}_4$  is actually transported and emitted at the peak of the melt period at the highest annual river discharge. As rivers and ocean shelves in the Arctic experience more abrupt collapses, erosion and thawing, this may contribute to the liberation and transport of soil-derived  $\text{CH}_4$ , resulting in the expansion of key areas and an increase in  $\text{CH}_4$  emissions into the atmosphere. Our results provide a

900 glimpse of the potential contribution of  $\text{CH}_4$  emissions from Arctic Rivers, adding up to the largely unknown contributions from permafrost and inland waters.

### Data availability

905 The hydrologic and gas data presented in this work will be made available through a link to the Zenodo public repository upon the publication of this work. All sequences of the microbial data have been deposited in GenBank with the reference BioProject No. PRJNA881395.

### Competing interests

910 The authors declare that they have no conflict of interest

Deleted: methane

Deleted: methane

Deleted: methane

Deleted: methane

Deleted: U

Deleted: river boundaries

Deleted: do not seem to be a source of

Deleted:  $\text{CH}_4$  into the Arctic Ocean via downstream transport with the river flow.

Deleted: Certainly, m

Deleted: of the Arctic Ocean

Deleted: shelves

Deleted: into the ocean

Deleted: ,

Deleted: as well as subsequent

Deleted: methane

### Author contribution

930 K.C.-M. conceived and designed the study. K.C.-M, A.C., A.K., K.K., S.A., O.K. and N.Z.  
contributed to fieldwork and logistics. K.C.-M, A.C., M.G., S.A., W.A.O. contributed to lab  
work, sample and data analyses. K.C.-M., A.C. and W.A.O wrote the paper with contributions  
from all authors in draft versions prior to submission.

### Acknowledgments

935 This work was conceived within the project PROPERAQUA funded by the Deutsche  
Forschungsgemeinschaft (DFG, German Research Foundation) (project No. 396657413). The  
contributions from AC and AK were funded by the MOSES program of the Helmholtz  
Association and the C-CASCADES ITN of the EU (project No. 643052). KK and WAO were  
940 supported by the Collaborative Research Centre 1076 AquaDiva (CRC AquaDiva) funded by  
DFG (project No. ID 218627073). MG and OK were supported through funding by the  
European Commission (INTAROS project, H2020-BG-09-2016, Grant Agreement No.  
727890, Nunataryuk project, H2020-BG-11-2016/17, Grant Agreement No. 773421).  
945 Especial thanks to the Northeast Scientific Station and the Pleistocene Park in Chersky for  
their invaluable assistance during fieldwork. Thanks to Dr. Robert Lehmann for the analysis  
of TOC samples at the FSU-Jena.

Deleted: D

## References

- 950 AMAP, Snow, water, ice and permafrost in the Arctic (SWIPA), In, Oslo, Norway, 269, 2017.
- Amorocho, J. and Devries, J. J.: A new evaluation of the wind stress coefficient over water surfaces, *Journal of Geophysical Research*, 85, 433-442, 10.1029/JC085iC01p00433, 1980.
- 955 Bogard, J. M., del Giorgio, P. A., Boutet, L., Garcia Chavez, M. C., Prairie, Y. T., Merante, A., and Derry, A. M.: Oxidic water column methanogenesis as major component of aquatic CH<sub>4</sub> fluxes, *Nature Communications*, 5, 5250, 10.1038/ncomms6350, 2014.
- Bring, A., Fedorova, I., Dibike, Y., Hinzman, L., Mård, J., Mernild, S. H., Prowse, T. D., Semenova, O., Stuefer, S. L., and Woo, M.-K.: Arctic terrestrial hydrology: a synthesis of processes, regional effects, and research challenges, *Journal of Geophysical Research: Biogeosciences*, 121, 621-649, 10.1002/2015JG003131, 2016.
- 960 Bussmann, I.: Distribution of methane in the Lena Delta and Buor-Khaya Bay, Russia, *Biogeosciences*, 10, 4641-4652, 10.5194/bg-10-4641-2013, 2013.
- Bussmann, I., Hackbusch, S., Schaal, P., and Wichels, A.: Methane distribution and oxidation around the Lena Delta in summer 2013, *Biogeosciences*, 14, 4985-5002, 10.5194/bg-14-4985-2017, 2017.
- 965 Campeau, A. and del Giorgio, P. A.: Patterns in CH<sub>4</sub> and CO<sub>2</sub> concentrations across boreal rivers: major drivers and implications for fluvial greenhouse emissions under climate change scenarios, *Global Change Biology*, 20, 1075-1088, 10.1111/gcb.12479, 2014.
- Canning, A., Körtzinger, A., Fietzek, P., and Rehder, G.: Technical note: seamless gas measurements across Land-Ocean Aquatic Continuum - corrections and evaluation of sensor data for CO<sub>2</sub>, CH<sub>4</sub> and O<sub>2</sub> from field deployments in contrasting environments, *Biogeosciences*, 18, 1351-1373, 10.5194/bg-18-1351-2021, 2021a.
- 970 Canning, A., Wehrli, B., and Körtzinger, A.: Methane in the Danube Delta: the importance of spatial patterns and diel cycles for atmospheric emissions estimates, *Biogeosciences*, 18, 3961-3979, 10.5194/bg-18-3961-2021, 2021b.
- 975 Castro-Morales, K., Canning, A., Körtzinger, A., Göckede, M., Küsel, K., Overholt, W. A., Wichard, T., Redlich, S., Arzberger, S., Kolle, O., and Zimov, N.: Effects of reversal of water flow in an Arctic stream on fluvial emissions of CO<sub>2</sub> and CH<sub>4</sub>, *Journal of Geophysical Research: Biogeosciences*, 127, e2021JG006485, 10.1029/2021JG006485, 2022.
- 980 Charkin, A. N., M. R. v. d. L., Shakhova, N. E., Gustafsson, Ö., Dudarev, O. V., Cherepnev, M. S., Salyuk, A. N., Koshurnikov, A. V., Spivak, E. A., Gunar, A. Y., Ruban, A. S., and Semiletov, I. P.: Discovery and characterization of submarine groundwater discharge in the Siberian Arctic seas: a case study in the Buor-Khaya Gulf, Laptev Sea, *The Cryosphere*, 11, 2305-2327, 10.5194/tc-11-2305-2017, 2017.
- 985 Chiasson-Poirier, G., Franssen, J., Lafrenière, M. J., Fortier, D., and Lamoureux, S. F.: Seasonal evolution of active layer thaw depth and hillslope-stream connectivity in a permafrost watershed, *Water Resources Research*, 56, 10.1029/2019WR025828, 2020.
- Connolly, C. T., Cardenas, M. B., Burkart, G. A., Spencer, R. G. M., and McClelland, J. W.:



- 990 Groundwater as a major source of dissolved organic matter to Arctic coastal waters, *Nature Communications*, 11, 1-8, 10.1038/s41467-020-15250-8, 2020.
- Crevecoeur, S., Vincent, W. F., Comte, J., and Lovejoy, C.: Bacterial community structure across environmental gradients in permafrost thaw ponds: methanotroph-rich ecosystems, *Frontiers in Microbiology*, 6, 192, 10.3389/fmicb.2015.00192, 2015.
- 995 Crevecoeur, S., Vincent, W. F., and Lovejoy, C.: Environmental selection of planktonic methanogens in permafrost thaw ponds, *Scientific Reports*, 6, 31312, 10.1038/srep31312, 2016.
- Crump, B. C., Peterson, B. J., Raymond, P. A., Amon, R. M. W., Rinehart, A., McClelland, J. W., and Holmes, R. M.: Circumpolar synchrony in big river bacterioplankton, *Proceedings of the National Academy of Sciences of the United States of America*, 106, 10.1073/pnas.0906149106, 2009.
- 1000 Dabrowski, J. S., Charette, M. A., Mann, P. J., Ludwig, S. M., Natali, S. M., Holmes, R. M., Schade, J. D., Powell, M., and Henderson, P. B.: Using radon to quantify groundwater discharge and methane fluxes to a shallow, tundra lake on the Yukon Kuskokwim Delta, Alaska, *Biogeochemistry*, 148, 69-89, 10.1007/s10533-020-00647-w, 2020.
- 1005 Dean, J. F., Meisel, O. H., Martyn, R. M., Beileli, L. M., Garnett, M. H., Lenderink, H., van Logtestijn, R., Borges, A. V., Bouillon, S., Lambert, T., Röckmann, T., Maximov, T., Petrov, R., Karsanaev, S., Aerts, R., van Huissteden, J., Vonk, J. E., and Dolman, A. J.: East Siberian Arctic inland waters emit mostly contemporary carbon, *Nature Communications*, 11, 1627, 10.1038/s41467-020-15511-6, 2020.
- 1010 Dean, J. F., Middelburg, J. J., Röckmann, T., Aerts, R., Blauw, L. G., Egger, M., Jetten, M. S. M., de Jong, A. E. E., Meisel, O. H., Rasigraf, O., Slomp, C. P., in't Zandt, M. H., and Dolman, A. J.: Methane feedbacks to the global climate system in a warmer world, *Reviews of Geophysics*, 56, 1-44, 10.1002/2017RG000559, 2018.
- Dlugokencky, E. and Tans, P. P.: [www.esrl.noaa.gov/gmd/ccgg/trends/](http://www.esrl.noaa.gov/gmd/ccgg/trends/), 2020.
- 1015 Downing, B. D., Pellerin, B. A., Bergamaschi, B. A., Saraceno, J. F., and Kraus, T. E. C.: Seeing the light: the effects of particles, dissolved materials, and temperature on in situ measurements of DOM fluorescence in rivers and streams, *Limnology and Oceanography: Methods*, 10, 767-775, 10.4319/lom.2012.10.767, 2012.
- Encinas Fernández, J., Peeters, F., and Hofmann, H.: On the methane paradox: transport from shallow water zones rather than in situ methanogenesis is the major source of CH<sub>4</sub> in the open surface water of lakes, *Journal of Geophysical Research: Biogeosciences*, 121, 2717-2726, 10.1002/2016JG003586, 2016.
- 1020 Etminan, M., Myhre, G., Highwood, E. J., and Shine, K. P.: Radiative forcing of carbon dioxide, methane, and nitrous oxide: a significant revision of the methane radiative forcing, *Geophysical Research Letters*, 43, 12614-12623, 10.1002/2016GL071930, 2016.
- 1025 Grossart, H.-P., Frindte, K., Dziallas, C., Eckert, W., and Tang, K. W.: Microbial methane production in oxygenated water column of an oligotrophic lake, *Proceedings of the National Academy of Sciences of the United States of America*, 108, 19657-19661, 10.1073/pnas.1110716108, 2011.

- 1030 Harms, T. K., Rocher-Ros, G., and Goodsey, S. E.: Emission of greenhouse gases from water tracks draining Arctic hillslopes, *Journal of Geophysical Research: Biogeosciences*, 125, e2020JG005889, 10.1029/2020JG005889, 2020.
- IPCC, Climate Change 2014: Synthesis Report. Contribution of Working Groups I, II and III to the Fifth Assessment Report of the Intergovernmental Panel on Climate Change, In, 1035 Geneva, Switzerland, 151, 2014.
- Kaiser, K., Canedo-Oropeza, M., McMachon, R., and Amon, R. M. W.: Origins and transformations of dissolved organic matter in large Arctic rivers, *Scientific Reports*, 7, 1-11, 10.1038/s41598-017-12729-1, 2017.
- 1040 Karlsson, J., Serikova, S., Vorobyev, S. N., Rocher-Ros, G., Denfeld, B. A., and Pokrovsky, O. S.: Carbon emission from Western Siberian inland waters, *Nature Communications*, 12, 1-8, 10.1038/S41467-021-21054-1, 2021.
- Kling, G. W., Kipphut, G. W., and Miller, M. C.: The flux of CO<sub>2</sub> and CH<sub>4</sub> from lakes and rivers in arctic Alaska, *Hydrobiologia*, 240, 23-26, 10.1007/BF00013449, 1992.
- 1045 Kwon, M. J., Beulig, F., Ilie, I., Wildner, M., Küsel, K., Merbold, L., Mahecha, M. D., Zimov, N., Zimov, S., Heimann, M., Schuur, E. A., Kostka, J. E., Kolle, O., Hilke, I., and Göckede, M.: Plants, microorganisms, and soil temperatures contribute to a decrease in methane fluxes on a drained Arctic floodplain, *Global Change Biology*, 23, 2396-2412, 10.1111/gcb.13558, 2017.
- 1050 Lammers, R. B., Shiklomanov, A. I., Vörösmarty, C. J., Fekete, B. M., and Peterson, B. J.: Assessment of contemporary Arctic river runoff based on observational discharge records, *Journal of Geophysical Research*, 106, 3321-3334, 10.1029/2000JD900444, 2001.
- 1055 Mann, P. J., Strauss, J., Palmtag, J., Dowdy, K., Ogneva, O., Fuchs, M., Bedington, M., Torres, R., Polimene, L., Overduin, P. P., Mollenhauer, G., Grosse, G., Rachold, V., Sobczak, W. V., Spencer, R. G. M., and Juhls, B.: Degrading permafrost river catchments and their impact on Arctic Ocean nearshore processes, *Ambio*, 51, 439-455, 10.1007/s13280-021-01666-z, 2022.
- Mansour, I., Heppell, C. M., Ryo, M., and Rilling, M. C.: Application of the microbial community coalescence concept to riverine networks, *Biological Reviews of the Cambridge Philosophical Society*, 93, 1832-1845, 10.1111/brv.12422, 2018.
- 1060 Mincer, T. J. and Aicher, A. C.: Methanol production by a broad phylogenetic array of marine phytoplankton, *PLoS ONE*, 11, e0150820, 10.1371/journal.pone.0150820, 2016.
- Olefeldt, D., Turetsky, M. R., Crill, P. M., and McGuire, A. D.: Environmental and physical controls on northern terrestrial methane emissions across permafrost zones, *Global Change Biology*, 19, 589-603, 10.1111/gcb.12071, 2013.
- 1065 Olid, C., Zannella, A., and Lau, D. C. P.: The role of methane transport from the active layer in sustaining methane emissions and food chains in subarctic ponds, *Journal of Geophysical Research: Biogeosciences*, 126, e2020JG005810, 10.1029/2020JG005810, 2021.
- 1070 Peeters, F. and Hofmann, H.: Oxidic methanogenesis is only a minor source of lake-wide diffusive CH<sub>4</sub> emissions from lakes, *Nature Communications*, 12, 1206, 10.1038/s41467-021-21215-2, 2021.

- Raymond, P. A., Zappa, C. J., Butman, D., Bott, T. L., Potter, J. D., Mulholland, P., Laursen, E., McDowell, W. H., and Newbold, D.: Scaling the gas transfer velocity and hydraulic geometry in streams and small rivers, *Limnology and Oceanography: fluids and environments*, 2, 41-53, 10.1215/21573689-1597669, 2012.
- 1075 Rosentreter, J. A., Borges, A. V., Deemer, B. R., Holgerson, M. A., Liu, S., Song, C., Melack, J. M., Raymond, P. A., Duarte, C. M., Allen, G. H., Olefeldt, D., Poulter, B., Battin, T. I., and Eyre, D.: Half of global methane emissions come from highly variable aquatic ecosystem sources, *Nature Geoscience*, 14, 225-230, 10.1038/s41561-021-00715-2, 2021.
- 1080 Saunois, M., Stavert, A. R., Bousquet, P., Canadell, J. G., and et al.: The global methane budget 2000-2017, *Earth System Scientific Data*, 12, 1561-1623, 10.5194/essd-12-1561-2020, 2020.
- 1085 Schuur, E. A., McGuire, D., Schädel, C., Grosse, G., Harden, J. W., Hayes, D. J., Hugelius, G., Koven, C. D., Kuhry, P., Lawrence, D. M., Natali, S. M., Olefeldt, D., Romanovsky, V. E., Schaefer, K., Turetsky, M. R., Treat, C. C., and Vonk, J. E.: Climate change and the permafrost carbon feedback, *Nature*, 520, 171-179, 10.1038/nature14338, 2015.
- Shakhova, N. and Semiletov, I. P.: Methane release and coastal environment in the East Siberian Arctic shelf, *Journal of Marine Systems*, 66, 227-243, 10.1016/j.jmarsys.2006.06.006, 2007.
- 1090 Shakirov, R. B., Mau, S., Mishukova, G. I., Obzhurov, A. I., Shakirova, M. V., and Mishukova, O. V.: The features of methane fluxes in the western and eastern Arctic: a review. Part I, *Geosystems of Transition Zones*, 4, 004-025, 10.30730/2541-8912.2020.4.1.004-025, 2020.
- 1095 Snyder, L., Potter, J. D., and McDowell, W. H.: An evaluation of nitrate, fDOM, and turbidity sensors in New Hampshire Streams, *Water Resources Research*, 54, 2466-2479, 10.1002/2017WR020678, 2018.
- Stanley, E. H., Casson, N. J., Christel, S. T., Crawford, J. T., Loken, L. C., and Oliver, S. K.: The ecology of methane in streams and rivers: patterns, controls, and global significance, *Ecological Monographs*, 86, 146-171, 10.1890/15-1027, 2016.
- 1100 Striegl, R. G., Dornblaser, M. M., McDonald, C. P., Rover, J. R., and Stets, E. G.: Carbon dioxide and methane emissions from the Yukon River System, *Global Biogeochemical Cycles*, 26, GB0E05, 10.1029/2012GB004306, 2012.
- 1105 Turetsky, M. R., Abbott, B. W., Jones, M. C., Walter Anthony, K., Olefeldt, D., Schuur, E. A., Grosse, G., Kuhry, P., Hugelius, G., Koven, C., Lawrence, D. M., Gibson, C., Sannel, A. B., and McGuire, D.: Carbon release through abrupt permafrost thaw, *Nature Geoscience*, 13, 138-143, 10.1038/s41561-019-0526-0, 2020.
- Vigneron, A., Cruaud, P., Bhiry, N., Lovejoy, C., and Vincent, W. F.: Microbial community structure and methane cycling potential along a thermokarst pond-peatland continuum, *Microorganisms*, 7, 10.3390/microorganisms7110486, 2019.
- 1110 Vorobyev, S. N., Karlsson, J., Kolesnichenko, Y. Y., and Koretz, M.: Fluvial carbon dioxide emission from the Lena River basin during spring flood, *Biogeosciences Discussions*, doi: 10.5194/bg-2021-109, 2021. 10.5194/bg-2021-109, 2021.

- Wanninkhof, R.: Relationship between gas exchange and wind speed over the ocean, *Journal of Geophysical Research*, 97, 7373-7381, 10.1029/92JC00188, 1992.
- 1115 Wanninkhof, R.: Relationship between wind speed and gas exchange over the ocean revisited, *Limnology and Oceanography: Methods*, 12, 351-362, 10.4319/lom.2014.12.351, 2014.
- Watras, C. J., Hanson, P. C., Stacy, T. L., Morrison, K. M., Mather, J., Hu, Y.-H., and Milewski, P.: A temperature compensation method for CDOM fluorescence sensors in freshwater, *Limnology and Oceanography Methods*, 9, 296-301, 10.4319/lom.2011.9.296, 2011.
- 1120 Weiss, R. F.: The solubility of nitrogen, oxygen and argon in water and sea water, *Deep Sea Research*, 17, 721-735, 10.1016/0011-7471(70)90037-9, 1970.
- Wiesenburg, D. A. and Guinasso, J. N. L.: Equilibrium solubilities of methane, carbon monoxide, and hydrogen in water and sea water, *Journal of Chemical and Engineering Data*, 24, 356-360, 10.1021/cr60306a003, 1979.
- 1125 Wik, M., Varner, R. K., Walter Anthony, K., MacIntyre, S., and Bastviken, D.: Climate-sensitive northern lakes and ponds are critical components of methane release, *Nature Geoscience*, 9, 99-106, 10.1038/NGEO2578, 2016.
- Xin, J., Zhang, Y., Zhang, S., Xia, C., and Li, S.: Methanol production from CO<sub>2</sub> by resting cells of the methanotrophic bacterium *Methylosinus trichosporium* IMV 3011, *Journal of Basic Microbiology*, 47, 426-435, 10.1002/jobm.200710313, 2007.
- 1130 Zolkos, S., Tank, S. E., Striegl, R., and Kokelj, S. V.: Thermokarst effects on carbon dioxide and methane fluxes in streams on the Peel Plateau (NWT, Canada), *Journal of Geophysical Research: Biogeosciences*, 124, 1781-1798, 10.1029/2019JG005038, 2019.
- 1135

## Figure Captions

**Figure 1** – Navigated transects in the Kolyma River: upstream (UP) (grey line, sampled from 15 June 2019 at 12:30 h to 16 June 2019 at 16:59 h) and downstream (DOWN) (black line, navigated on 16-17 June 2019). Gaps in the continuous UP and DOWN transects are data not considered for the analysis because they involved navigation outside the main river channel (i.e., transects at Leonid's stream and the Ambolikha River indicated in red). Discrete samples were collected in 21 sampling stations (PP05-PP25) during the UP transect (grey markers). Key sites (and stations): S1 (PP07), S2 (PP11), S3 (PP20), S4 (PP23), and S5 (PP25) are circled in yellow. This map was created using MATLAB® with data from a composite image for June, July and August from 2015-2018 using Sentinel-2 NDVI maps (<https://developers.google.com/earth-engine/datasets/catalog/sentinel>).

**Figure 2** – Spatial distribution of water properties measured along transects UP (left) and DOWN (right) at the main stem of the Kolyma River for  $p\text{CH}_4$  (a and b),  $T$  (c and d), and  $\kappa$  (e and f). The location of key sites S1 to S5 are indicated. The values corresponding to Ambolikha River and Leonid's stream are not shown.

**Figure 3** – Water properties measured in transects UP (grey) and DOWN (black): a) water temperature,  $T$ ; b) water-specific conductivity,  $\kappa$ ; c)  $\text{CH}_4$  concentration,  $C_w$ , and d) flux density of  $\text{CH}_4$ ,  $\text{FCH}_4$ , all shown as a function of the navigated distance (km) along each transect. The location corresponding to the key sites S1 to S5 are indicated and color-coded in each signal (light grey – UP transect and black – DOWN transect). The Ambolikha River and Leonid's stream are shown in red. Gaps in the data indicate erroneous or not measured data in the transect.

**Figure 4** – Correlation graphs for UP (a and b) and DOWN (c and d) transects between  $T$ ,  $\kappa$  and  $p\text{CH}_4$  as a function of the distance to bank ( $z$  in km) indicated in the color scale.

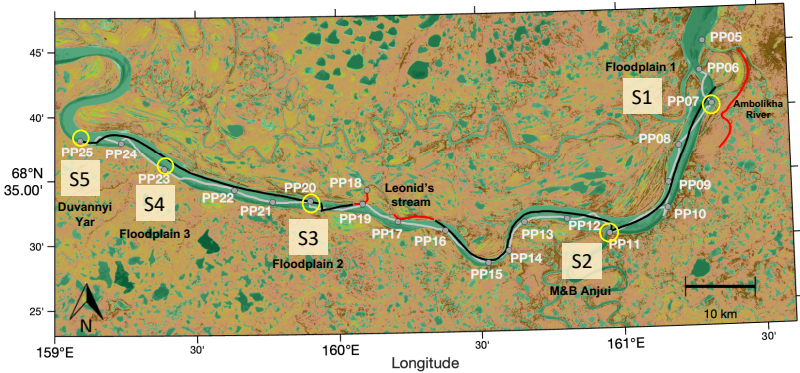
**Figure 5** – Riverine microbial community composition linked to temperature (left) and specific conductivity (right). Both plots represent the same underlying community data, with dissimilarities determined by the Bray-Curtis metric and visualized with non-metric multidimensional scaling plots.

**Figure 6** – Relative (top) and pseudo-absolute (bottom) abundances of putatively methanogenic archaeal genera (left) and methylotrophic bacterial families (right). An expanded version that includes only the methanotrophs is available in the supplemental information.

**Figure 7** – Linear correlations between the total absolute abundances of archaeal microbial communities (left, methanogens and right, methanotrophs) and the 1-min averages of water properties measured at the 21 sampling stations along the DOWN transect in Kolyma River. Red numbers in some of the markers indicate the station number corresponding to the key sites S1 to S5.

**Figure 8** – Average flux density of  $\text{CH}_4$  ( $\text{FCH}_4$ ) calculated for the entire UP and DOWN transects, and for the key sites and other sites.  $\text{FCH}_4$  for the tributaries Ambolikha River and Leonid's stream are also shown. Error bars denote the standard deviation of the mean.

**Fig. 1**



1190

1195

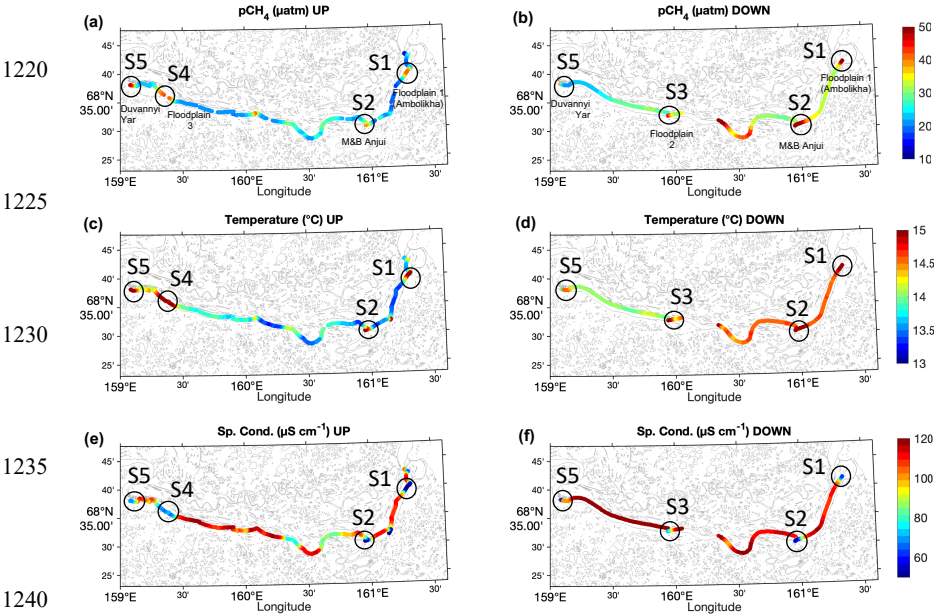
1200

1205

1210

1215

Fig. 2



1245

1250

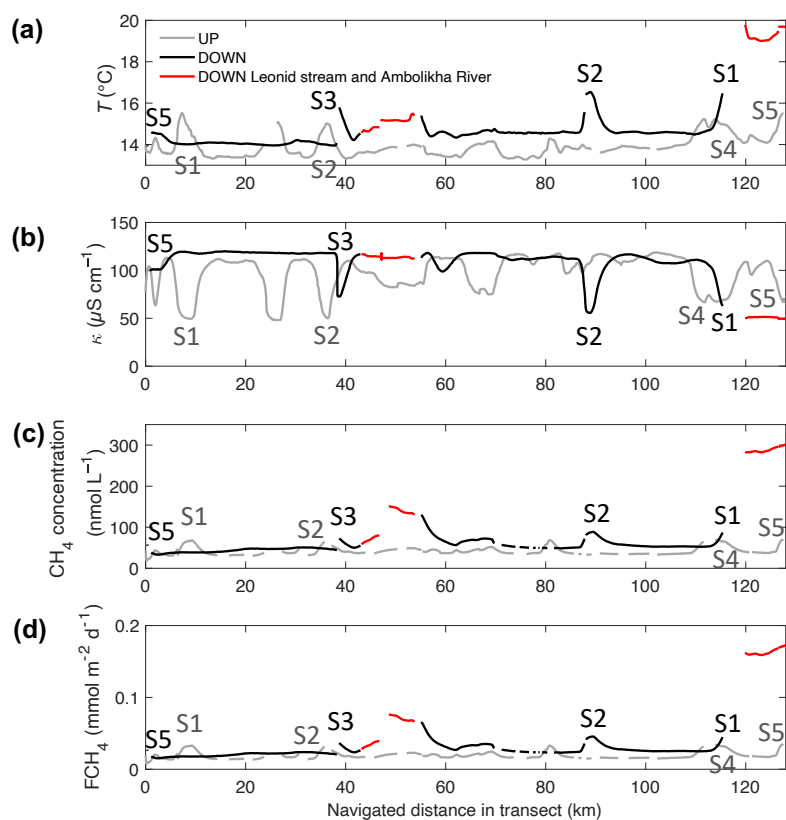
1255

1260

1265

**Fig. 3**

Water properties measured along the UP and DOWN transect in Kolyma River (15-17 June 2019)



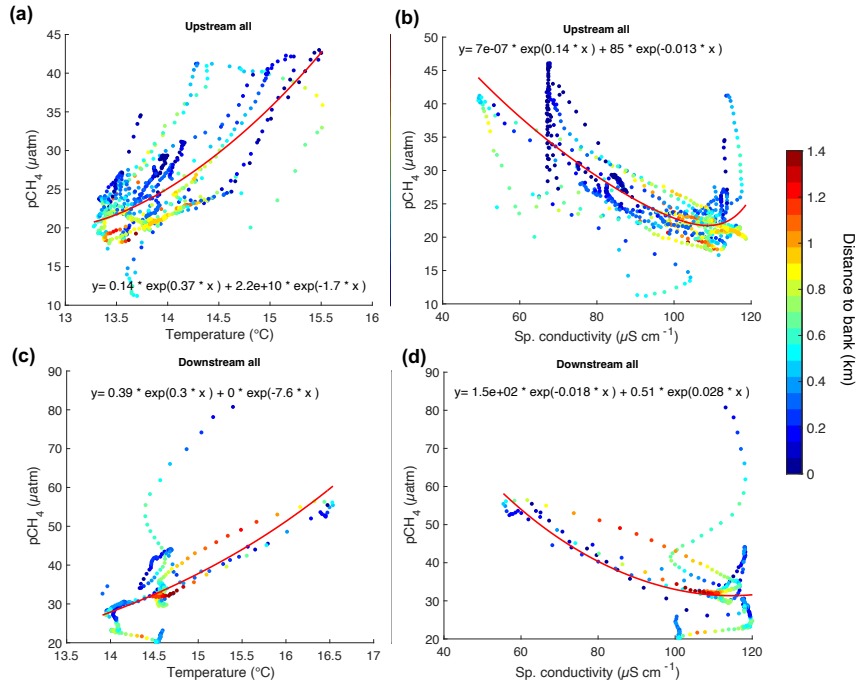
1270

1275

1280

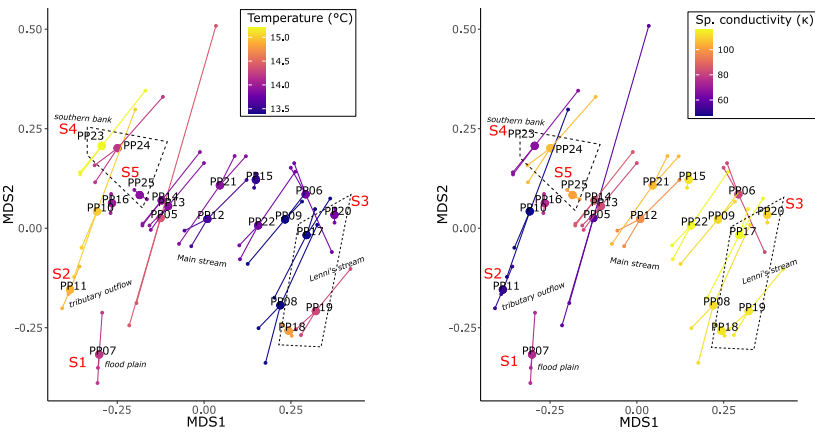


**Fig. 4**



1310

Fig. 5



1315

1320

1325

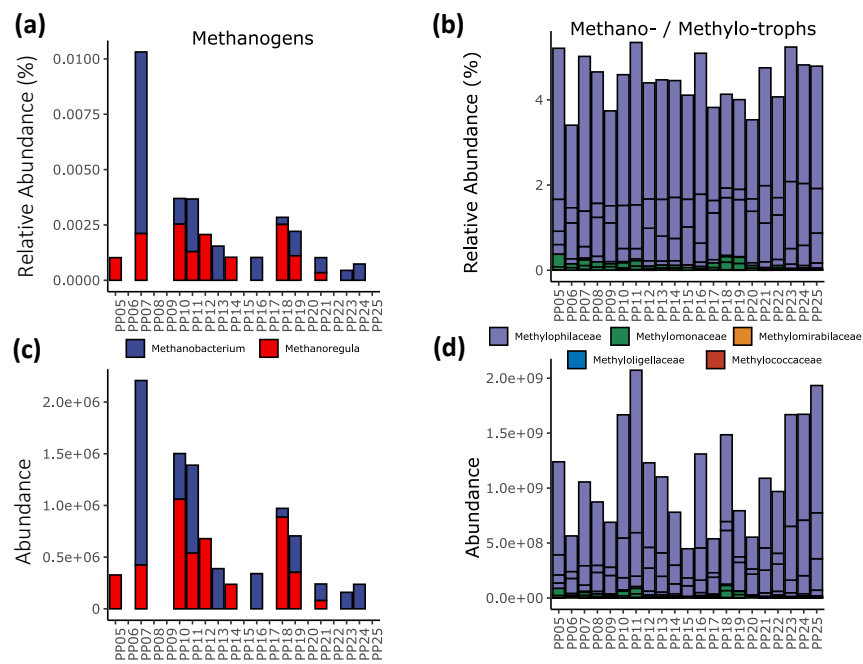
1330

1335

1340

1345

Fig. 6



1350

1355

1360

1365

1370

Fig. 7

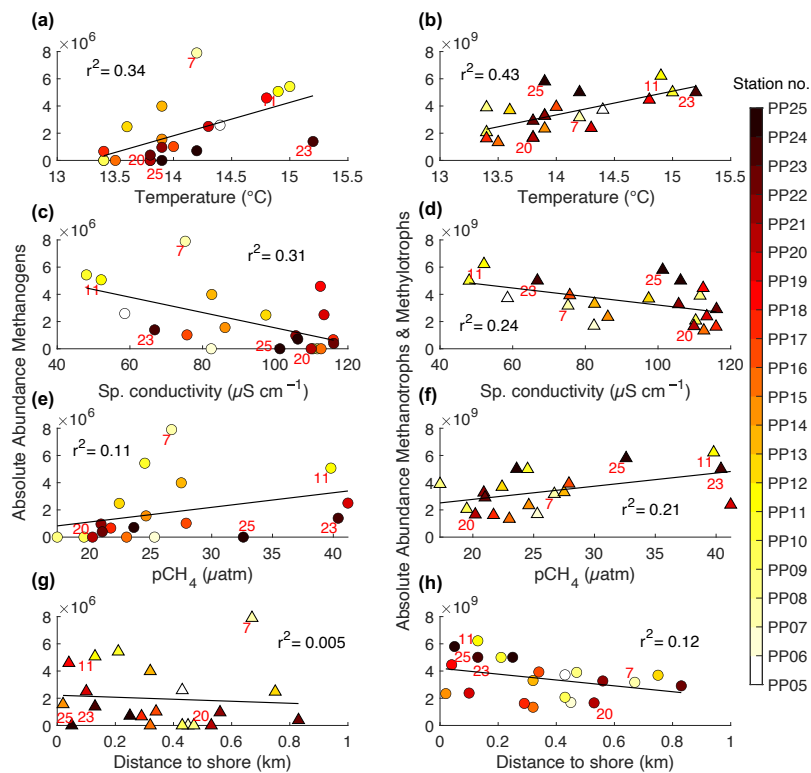
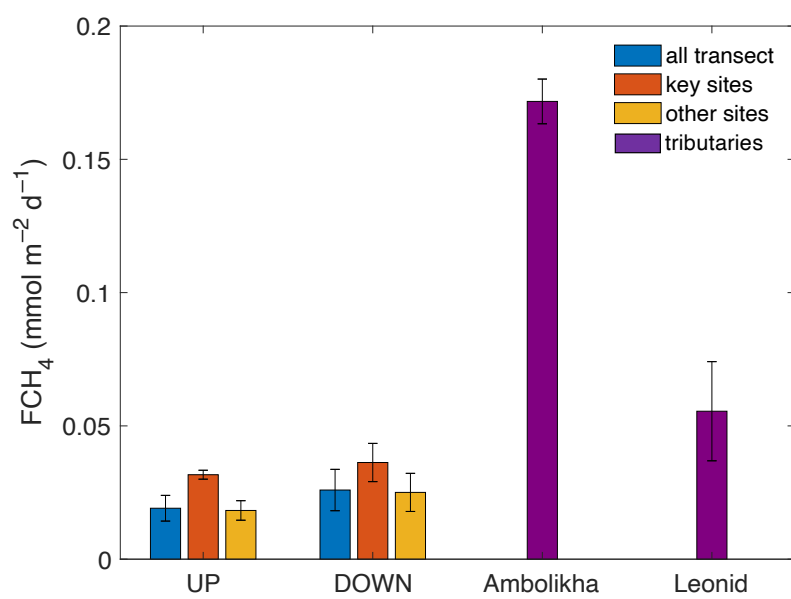


**Fig. 8**



1395

1400

**Table 1** – Average  $\pm$  1 std. deviation (minimum and maximum values below it) of  $p\text{CH}_4$ , the concentration of  $\text{CH}_4$  ( $C_w$ ),  $T$  and  $\kappa$  measured along the UP and DOWN transects in key sites (S1 – S5) and in the other sites of each transect. Measurements done in a tributary (Ambolikha River) and a stream (Leonid's stream) as part of the measurements during the DOWN transect are also shown.

Location	$p\text{CH}_4$ ( $\mu\text{atm}$ )	$C_w$ ( $\text{nmol L}^{-1}$ )	$T$ ( $^{\circ}\text{C}$ )	$\kappa$ ( $\mu\text{S cm}^{-1}$ )
Both transects	28.3 $\pm$ 8.5 (11.2 – 80.7)	45.9 $\pm$ 12.9 (18.9 – 130.2)	14.1 $\pm$ 0.6	96.8 $\pm$ 21.5
UP transect	25.8 $\pm$ 6.7 (11.2 – 46.1)	41.5 $\pm$ 9.2 (18.9 – 69.2)	13.9 $\pm$ 0.6	92.2 $\pm$ 22.2
UP key sites	39.4 $\pm$ 4.3	65.0 $\pm$ 3.0	14.9 $\pm$ 0.3	65.1 $\pm$ 6.9
UP other sites	23.8 $\pm$ 4.3	39.9 $\pm$ 7.0	13.9 $\pm$ 0.5	95.8 $\pm$ 20.9
DOWN transect	33.2 $\pm$ 9.4 (20.2 – 80.7)	54.3 $\pm$ 14.7 (33.3 – 130.2)	14.5 $\pm$ 0.5	108.3 $\pm$ 14.5
DOWN key sites	42.8 $\pm$ 9.2	72.4 $\pm$ 12.4	15.7 $\pm$ 0.8	76.0 $\pm$ 16.0
DOWN other sites	31.8 $\pm$ 8.5	52.7 $\pm$ 13.7	14.4 $\pm$ 0.3	112.4 $\pm$ 7.3
Ambolikha River (DOWN)	206.8 $\pm$ 9.8 (191.7 – 222.9)	300.7 $\pm$ 12.1 (282.2 – 320.7)	19.6 $\pm$ 0.3	49.9 $\pm$ 0.9
Leonid's stream (DOWN)	66.8 $\pm$ 22.0 (37.0 – 92.9)	111.1 $\pm$ 35.7 (60.8 – 150.7)	15.1 $\pm$ 0.3	113.9 $\pm$ 1.6

1405